Published in final edited form as:
Bone. 2005 January ; 36(1): 33–46. doi:10.1016/j.bone.2004.09.015.

Surface plasmon resonance (SPR) confirms that MEPE binds to PHEX via the MEPE–ASARM motif: a model for impaired mineralization in X-linked rickets (HYP)

Peter S.N. Rowe[a,*], **Ian R. Garrett**[b], **Patricia M. Schwarz**[c], **David L. Carnes**[a], **Eileen M. Lafer**[c], **Gregory R. Mundy**[b,d], and **Gloria E. Gutierrez**[b]

[a]Department of Periodontics, University of Texas Health Science Center at San Antonio, San Antonio, TX, 78229, USA

[b]Osteoscreen, San Antonio, TX 78229, USA

[c]Department of Biochemistry, University of Texas Health Science Center at San Antonio, San Antonio, TX, 78229, USA

[d]Department of Cellular and Structural Biology, University of Texas Health Science Center at San Antonio, San Antonio, TX, 78229, USA

Abstract

Matrix ***E***xtracellular ***P***hospho-glycoprot***E***in (MEPE) and proteases are elevated and PHEX is defective in HYP. PHEX prevents proteolysis of MEPE and release of a protease-resistant MEPE–ASARM peptide, an inhibitor of mineralization (minhibin). Thus, in HYP, mutated PHEX may contribute to increased ASARM peptide release. Moreover, binding of MEPE by PHEX may regulate this process in normal subjects. The nature of the PHEX–MEPE nonproteolytic interaction(s) (direct or indirect) is/are unknown. Our aims were to determine (1) whether PHEX binds specifically to MEPE, (2) whether the binding involves the ASARM motif region, and (3) whether free ASARM peptide affects mineralization in vivo in mice. Protein interactions between MEPE and recombinant soluble PHEX (secPHEX) were measured using surface plasmon resonance (SPR). Briefly, secPHEX, MEPE, and control protein (IgG) were immobilized on a Biacore CM5 sensor chip, and SPR experiments were performed on a Biacore 3000 high-performance research system. Pure secPHEX was then injected at different concentrations, and interactions with immobilized proteins were measured. To determine MEPE sequences interacting with secPHEX, the inhibitory effects of MEPE–ASARM peptides (phosphorylated and nonphosphorylated), control peptides, and MEPE midregion RGD peptides on secPHEX binding to chip-immobilized MEPE were measured. ASARM peptide and etidronate-mediated mineralization inhibition in vivo and in vitro were determined by quenched calcein fluorescence in hind limbs and calvariae in mice and by histological Sanderson stain. A specific, dose-dependent and Zn-dependent protein interaction between secPHEX and immobilized MEPE occurs (EC_{50} of 553 nM). Synthetic MEPE PO_4-ASARM peptide inhibits the PHEX–MEPE interaction (K_{Dapp} = 15 uM and $B_{max/inhib}$ = 68%). In contrast, control and MEPE–RGD peptides had no effect. Subcutaneous administration of ASARM peptide resulted in marked quenching of fluorescence in calvariae and hind limbs relative to vehicle controls indicating impaired mineralization. Similar results were obtained with etidronate. Sanderson-stained calvariae also indicated a marked increase in unmineralized osteoid with ASARM peptide and etidronate groups. We conclude that PHEX and MEPE form a nonproteolytic protein interaction via the MEPE carboxy-terminal

*Corresponding author. Department Periodontics, The University of Texas Health Science Center at San Antonio, UTHSCSA, 7703 Floyd Curl Drive, Room 3.579U, San Antonio, TX 78229. Fax: +1 210 567 6858. rowep@uthscsa.edu (P.S.N. Rowe).

ASARM motif, and the ASARM peptide inhibits mineralization in vivo. The binding of MEPE and ASARM peptide by PHEX may explain why loss of functional osteoblast-expressed PHEX results in defective mineralization in HYP.

Keywords

PHEX; MEPE; Rickets; Osteomalacia; Mineralization

Introduction

Defects in two genes PHEX and FGF23 are primarily responsible for X-linked hypophosphatemic rickets (HYP) and autosomal dominant hypophosphatemic rickets (ADHR) [29,92]. The molecular pathways(s) and the upstream factors impacting on mineralization, abnormal renal phosphate handling, and vitamin D metabolism remain unknown. However, evidence strongly suggests that PHEX and FGF23 pathways overlap and may well involve the direct or indirect regulation of extracellular matrix proteins (ECMP) from bone and teeth [62,68,71]. ***M***atrix ***E***xtracellular ***P***hospho-glycoprot***E***in (MEPE), an osteoblast and odontoblast expressed matrix protein, is a good downstream candidate ECMP factor whose expression or activity may be altered by PHEX and/or FGF23. MEPE was first cloned from a patient with oncogenic hypophosphatemic osteomalacia (OHO), a disease with many similarities to HYP and ADHR. The OHO tumor cloning was achieved by expression screening of an OHO tumor cDNA library with polyclonal antibodies that neutralized an OHO tumor-secreted renal phosphate uptake inhibiting factor(s) [69,72]. MEPE is markedly up-regulated in Hyp osteoblasts and OHO tumors and is exclusively expressed in osteoblasts, osteocytes, and odontoblasts [2,3,25,27,31,45,60,61,69, 71,72]. MEPE inhibits phosphate uptake and mineralization in vivo and in vitro. Phosphaturia in rodents can be induced via bolus administration or infusion of recombinant MEPE [14,71]. The in vitro mineralization inhibition observed with MEPE is mediated by a short (2 kDa), protease-resistant, cathepsin B-released carboxy-terminal MEPE peptide (ASARM peptide) [69,71]. This peptide likely also inhibits phosphate uptake. Recently, based on our published findings, we proposed a mineralization model that involved a nonproteolytic sequestration of MEPE by PHEX [68,71]. Specifically, a reversible association of PHEX and MEPE was proposed to control release of a mineralization inhibitor ASARM peptide by transiently protecting MEPE from proteolysis. Also, in HYP, the reported massive up-regulation of MEPE, the excess protease expression, and the lack of functional PHEX should also collectively increase the levels of MEPE–ASARM peptide. This in turn was proposed to be responsible for the observed periosteocytic defects in mineralization [68,71].

PHEX belongs to an M13 family of Zn metalloendopeptidases, and its physiological substrate remains elusive. Although small synthetic peptides of FGF23 and MEPE are PHEX substrates, a number of studies have failed to confirm cleavage of the full-length molecules [12,27,39]. Interestingly, we previously determined that PHEX protects MEPE from cathepsin B proteolysis [27]. More specifically, both full-length PHEX and/or a mutated PHEX protein that contains the COOH terminal extracellular domain (with zinc binding motif) prevent cathepsin B degradation of full-length MEPE in vitro. Moreover, this inhibition is not mediated through PHEX proteolysis of cathepsin B, and cathepsin B does not degrade PHEX [27]. However, our published experiments did not examine whether the observed in vitro PHEX-dependent protection of MEPE was direct or indirect. Indeed, PHEX potentially could either form a nonproteolytic complex with cathepsin B, MEPE, or both proteins. Others have also shown that PHEX activity is inhibited by a nonproteolytic association with another important bone matrix protein, osteocalcin [6]. The data presented

in this study confirm that PHEX and MEPE do indeed form a specific, direct, Zn-dependent and nonproteolytic association. Moreover, the carboxy-terminal ASARM motif region of MEPE plays a key role in the MEPE–PHEX interaction. Finally, we confirm that the phosphorylated ASARM peptide quenches calcein bone fluorescence in vivo and increases the osteoid band in Sanderson-stained calvariae. This is consistent with the in vitro mineralization inhibition generated by MEPE, OPN, DMP-1, and statherin phosphorylated ASARM peptides or proteins [8,9,28,44,64,68,71,76,90]. The statherin ASARM peptide, for example, prevents ectopic mineralization of calcium and phosphate in supersaturated saliva and plays a key role in the mineralization dynamics of teeth [44,64,76]. The findings presented in this study are strongly supportive of the HYP mineralization ASARM model [68,69,71].

Materials and methods

Expression of insect-expressed MEPE and soluble mammalian-expressed PHEX (secPHEX)

Expression and purification of full-length insect-expressed human MEPE were as described previously [71]. Briefly, insect *S. frugiperda* cells were infected with baculovirus containing the full-length human MEPE gene originally cloned into pBlueBac-4-5 (cDNA) and homologously recombined with Bac-N-Blue DNA™ to generate viral particles via transfection (Invitrogen kit). Infected cells were grown in a 10-l bioreactor for 48 h, and conditioned medium was concentrated (fivefold) and used as the starting material for purification as previously described [71]. The final product integrity was verified by N-terminal sequence analysis and Western blot analyses using antibodies to the N-terminus, midregion, and C-terminus. Purified protein contained N-terminal amino acid residues APTFQ, confirming cleavage of predicted nascent-MEPE signal peptide by the *S. frugiperda* insect cells [71]. Thus, the purified Hu-MEPE protein consisted of the entire MEPE sequence minus the signal peptide (minus first 16 residues MRVFCVGLLLFSVTWA). The protein was not tagged with additional sequence [71]. Pure, mammalian-expressed human recombinant-secreted PHEX (secPHEX), was donated as a kind gift by Dr. Philippe Crine and Dr. Guy Boileau (Department of Biochemistry, University of Montreal) and was prepared as previously described [6,12]. Briefly, to generate a soluble, secreted form of PHEX, the signal peptide/membrane anchor domain (SA domain) of the protein was transformed into a cleavage-competent signal sequence using a strategy similar to that previously described for NEP [38], with modifications for secPHEX as described previously [6,12]. Purified secPHEX was also analyzed and validated by SDS/PAGE, Western blotting, and N-terminal sequence determined again as described previously [6,12].

Synthetic peptides

Four sets of peptides were synthesized using standard techniques and purchased from MPS Biosystems (Multiple Peptide Systems, Inc., San Diego, CA). Peptide purity was greater than 80% via HPLC, ion exchange, and also mass spectrometry. Three of the peptides were derived from MEPE sequence. One of the MEPE peptides was derivative of the midregion (residues 238 to 262) of MEPE and contained the RGD motif (MEPE–RGD). The other two MEPE peptides consisted of the last 19 COOH-terminal residues encompassing the ASARM motif (residues 507 to 525). One of the ASARM peptides was phosphorylated (PO_4-ASARM peptide), and the other was nonphosphorylated (ASARM peptide). All the peptide sequences are shown in Table 1. The MEPE–RGD (midregion) peptide served as negative control and did not competitively inhibit MEPE–PHEX interactions (see Results). The design of an ASARM scrambled peptide was not feasible due to the unique nature of the sequence. Specifically, the key characteristics of the motif are the enriched aspartic acid (D), serine (S), and glutamic acid residues (E), thus scrambling of the sequence would not

substantively alter the key physicochemical properties (i.e., low pI, high charge, acidic nature, and serine phosphorylation). To overcome this potential pitfall, as mentioned, the control peptide from another region of MEPE (MEPE–RGD) was used as a negative control.

Surface plasmon resonance (SPR)

A Biacore 3000 SPR instrument in conjunction with CM5 research grade chips was used to conduct the Surface Plasmon Resonance (SPR) experiments (Biacore, Piscataway, NJ) as previously described [52–54]. The experiments were performed at 25°C using Biacore buffer (10 mM HEPES pH 7.4, 150 mM NaCl, 0.005% surfactant P20) supplemented with 2 mM $ZnCl_2$ (HBS-P-Zn) or without $ZnCl_2$ (HBS-P) as indicated. Injected samples also contained 2 mg/ml carboxymethyl dextran to reduce nonspecific association with the dextran matrix of the chip, and a flow rate of 5 μl/min was used. The surfaces of research grade CM5 chips were activated by a 6-min injection of a solution containing 0.2 M *N*-ethyl-*N*9-(dimethylaminopropyl) carbodiimide and 0.05 M *N*-hydroxy-succinimide. MEPE, PHEX, and IgG were immobilized on the same chip (ligands) in different individual flow cells. Each chip contains four separate flow cells; one cell was left blank as a negative control. The experiments were repeated on two different chips with 3500 RU (response units) and 6000 RU of immobilized proteins respectively. The response unit or RU is a measure of surface charge density oscillation and surface plasmon-positron generation as detected by changes in incident refractive index monitored by the Biacore optical unit. Specifically, 1000 RU equals a change of approximately 1 ng/mm^2 in surface protein concentration on the chip surface. After immobilization, each surface was blocked by a 6-min injection of 1 M ethanolamine at pH 8.5. Following immobilization, PHEX (analyte) was passed over the surfaces for 6 min at the indicated concentrations in HBS-P-Zn or HBS-P buffer, followed by a 6-min dissociation. Surfaces were then regenerated by a 1-min injection of 6 M guanidine-HCl. Protein–protein interactions between analyte (PHEX) and immobilized ligand (MEPE, PHEX, or IgG) are reported as sensorgrams which are plots of RU versus time. An increase in RU reflects changes in the concentration of molecules at the surface of the sensor chip as a result of a specific interaction between analyte and ligand. The following equation was used to calculate EC_{50} from the Biacore sensorgram: RU = B_{max} × (secPHEX(uM))/EC_{50} + (secPHEX(uM)). The B_{max} value indicates the maximal RU (protein–protein interaction) achieved at saturation or high doses of secPHEX.

Surface plasmon resonance: synthetic peptides and competitive PHEX–MEPE binding studies

For these experiments, CM-5 chips containing flow cells immobilized with MEPE, PHEX and IgG ligands at 6000 RU were used. Just prior to SPR injection, stock solution of specific peptide (as defined for each experiment; see Table 1) and dissolved in analyte buffer (HBS-P-Zn) were added to a constant 250 nM PHEX analyte solution to give final peptide concentrations of either 0, 11, 22, 42, or 83 nM. In this way, a dose-dependent inhibition curve was calculated for each of the peptides and apparent K_D's calculated using solution competition (K_{Dapp}). The following equation was used to compute K_{Dapp} values: RU = $B_{max/inhib}$ × (peptide(uM))/K_{Dapp} + (peptide(uM)). The $B_{max/inh}$ value represents the maximal percentage inhibition change in RU (i.e., PHEX–MEPE binding) relative to the "nonpeptide" control (0% inhibition of binding), using a constant analyte flow solution of secPHEX of 250 nM against immobilized MEPE ligand at 6000 RU. Only the phosphorylated ASARM peptide (PO_4-ASARM peptide) and the nonphosphorylated ASARM peptide (ASARM peptide) were able to inhibit MEPE–PHEX interactions (see Results). The control MEPE–RGD peptide was ineffective.

Subcutaneous administration of PO_4-ASARM peptide, etidronate (EHDP), and calcein

Three separate groups of male ICR Swiss mice (4–5 weeks) were subcutaneously injected once a day (9:00 am), for 12 days except for days 6 and 7 with 50 μl solutions of either (1) etidronate (EHDP) (10 mg/kg/day), (2) PO_4-ASARM peptide (2 mg/kg/day), or (3) vehicle consisting of 5 mM HEPES pH 7.4/150 mM NaCL/0.1% BSA. The synthetic PO_4-ASARM peptide was dissolved in vehicle (1.0 mg/ml). Etidronate was first dissolved in 150 mM NaCl and then buffered to pH 7.5 with 1 M NaOH to give a 5 mg/ml solution. The 10 mg/kg/day doses of etidronate have previously been reported to inhibit mineralization in rats and were used as positive controls [7,85]. All three groups were subcutaneously injected with calcein (20 mg/kg/day) on days 3, 5, 9, and 11, respectively. The degree of calcein fluorescence and/or fluorescence quenching is an indicator of mineralization status (see next section). The calcein injections when given were administered 1 h after the daily injections of PO_4-ASARM peptide, EHDP, or vehicle. Animals were then terminated humanely, and calvariae plus femurs/tibia were fixed in 70% ethanol (nondecalcified). After fluorescence imaging (see Fig. 6), calvariae were processed in plastic and stained with Sanderson's stain (see below). Five animals per group were used for statistical analysis of fluorescence quenching and histological Sanderson staining.

Calcein fluorescence in mice calvariae, hind limbs, and fluor-imager analysis of mineralization

A Bio-Rad FluorMax fluor-imager was used to simultaneously image all the samples from each of the three groups (15 animals; 5 animals per group). This consisted of 10 tibia/femurs and 5 calvariae per group. Samples were placed on top of the fluor-imager platen contained within a light-tight box. Ultraviolet (UV) light was used to generate calcein-mediated epifluorescence, and the fluorescent image was captured on a −40°C, peltier-cooled, 1340 × 1040 pixel CCD resolution, CCD digital camera. Quantitation of fluorescence was carried out using Quantity-1, Bio-Rad, fluorescence software. Pixel saturation was prevented by internal software calibration and exposure adjustment. All fluorescence readings were thus accurately quantitative and nonsaturating. Photomicrographic UV fluorescent analysis of calvarial cross-sections embedded in plastic and mounted as slides (<100-μm sections) was also undertaken, and a description of the fixation and processing is given in the next section.

Sanderson staining and fluorescence detection of calvarial osteoid and mineralized bone

Staining of nondecalcified calvarial sections was performed using the method described by Sanderson and Bachus [75]. This technique provides excellent differential staining between unmineralized osteoid (blue) and mineralized bone (pink). Prior to staining, calvariae were dissected, and attached tissue was removed. Calvariae were then placed in 70% ethanol for further fixation as described [75]. After fixing and processing, undecalcified calvariae were embedded in plastic (LR-white acrylic resin (London Resin Co., Reading England)) as previously described [24]. Plastic embedded sections were ground to <100 μm using a specialized grinding pestle as described by Donath and Breuner [15]. Calcein fluorescence (indicator of mineralization; calcein binds to mineralizing bone) was then visualized using UV microscopy.

Statistics

Differences were assessed statistically by the use of Newman-Keuls or Bonferroni multiple comparison equations (as indicated) after one-way analysis of variance (nonparametric). A P value of less than 0.05 was considered significant. The standard error of the mean (SEM) was used as a representative measure of how far the sample mean differed from the true population mean. Quantity 1 Bio-Rad software was used to analyze the intensity of fluorescence emitted by epi-UV illumination of samples, and this was captured by a Bio-

Rad FluorMax digital imaging system and data incorporated into GraphPad Prizm-4 software (Graph-pad Software, Inc.), for statistical analysis as indicated.

Results

Specific Zn-dependent and dose-dependent direct binding of MEPE to PHEX

Fig. 1 shows a direct protein–protein Zn-dependent interaction between secPHEX and MEPE as monitored and plotted as an SPR sensorgram. A classic protein-association phase was followed by dissociation after the 6-min pulse of secPHEX. There were no significant signals generated between secPHEX and blank activated/blocked chip or control IgG protein. There was a very low-level barely detectable autologous interaction between injected secPHEX (analyte) and chip-immobilized secPHEX (ligand). The strong MEPE–PHEX interaction was dose-dependent (see Fig. 2) with an EC_{50} = 553 nM (concentration of MEPE required to reach half-maximal binding or RU units). Figs. 3a and b graphically illustrate the dose-dependent PHEX–MEPE binding derived from the Biacore sensorgram shown in Fig. 1. No interaction was observed between MEPE and PHEX in buffer lacking $ZnCl_2$ (HBS-P) in concentrations of secPHEX analyte up to 10 uM. Thus, MEPE specifically binds to PHEX in a dose-dependent, Zn-dependent, and saturable manner indicative of a ligand–receptor interaction following the law of mass action.

MEPE–ASARM peptides competitively inhibit binding of PHEX to MEPE

Premixing of PO_4-ASARM peptide or ASARM peptide with secPHEX prior to injection resulted in a dramatic dose-dependent inhibition of MEPE–PHEX protein–protein interaction (see Fig. 4). The MEPE–PHEX binding also reached saturation at high doses of secPHEX as shown in the SPR sensorgram (Fig. 4). An apparent K_{Dapp} of 15 υM was calculated for the PO_4-ASARM peptide with a binding maximal inhibition ($B_{max/inh}$) of 68% (see Figs. 5a and b). The calculated $B_{max/inh}$ value represents the peptide-mediated, maximal percentage inhibition of MEPE–PHEX binding relative to the nonpeptide control (0% inhibition). This value was determined using a constant analyte flow solution of 250 nM secPHEX against immobilized MEPE ligand at 6000 RU. The unphosphorylated ASARM peptide was less effective at competitively inhibiting the MEPE–PHEX interaction with an apparent K_{Dapp} of approximately 35 υM (graph not shown) compared to 15 υM for PO_4-ASARM peptide (Figs. 4 and 5). There was no inhibition of PHEX–MEPE interaction detected at high and low concentrations (up to 85 uM) of control MEPE–RGD peptide under identical secPHEX premixing conditions (data not shown).

ASARM peptide and etidronate mediated in vivo quenching of calcein fluorescence

UV induced calcein epifluorescence in dissected calvariae, tibiae and femurs was quenched significantly and markedly in both ASARM peptide (experimental) and etidronate (positive control) and groups compared to vehicle. Fig. 6 dramatically illustrates the fluorescence quenching of calvariae and hind limbs (imaged simultaneously) as captured using a cooled digital camera (Bio-Rad FluorImager Max system). The nonsaturated fluorescence was quantitated using quantity-1 imaging software (Bio-Rad) and the graphical results for calvariae and tibia/femurs are shown in Figs. 7a,b. A significant drop in calvarial fluorescence of 62% ($P < 0.001$) in PO_4-ASARM peptide and 48% ($P < 0.01$) in the etidronate group was measured relative to vehicle (see Figs. 7a and b for statistics and graph). A similar marked quenching also occurred with tibia/femur and the PO_4-ASARM peptide group with fluorescent intensity reduced by 44.5% ($P < 0.01$) relative to vehicle (Fig. 7b). The quenching of fluorescence in the etidronate group was expected. This is because etidronate potently inhibits mineralization in man and rodents at the levels administered [7,46,47,85]. The quenching in the ASARM group was even more marked than

the etidronate group in both calvariae and femurs/tibia confirming a major ASARM peptide inhibition of mineralization in vivo.

Absence of lamellar fluorescence bands in calvarial cross-sections of ASARM peptide and etidronate groups

Fig. 8 depicts representative UV-fluorescent photomicrographs of calvarial cross-sections from vehicle, etidronate, and ASARM peptide groups. Four distinct lamellar fluorescent layers representing the four separate calcein injections (20 mg/kg/day) are clearly visible in the vehicle group. The fluorescent bands represent calcein binding to actively mineralizing bone surface. In contrast, there is a complete absence of these layers in the ASARM peptide- and etidronate-treated groups. This strongly suggests that mineralization is inhibited by the addition of ASARM peptide and, as expected, by etidronate in vivo. These results are in agreement with the whole fluorescence imaging of calvariae and tibiae/femurs described above.

Sanderson's osteoid staining is increased in calvarial sections of ASARM and etidronate groups

Nondecalcified sections of calvariae from PO_4-ASARM peptide- and etidronate-treated groups showed marked increase in osteoid in calvarial cross-sections compared to the vehicle group (Fig. 9). Sanderson histological staining colors mineralized bone pink and nonmineralized matrix or osteoid blue [75]. Fig. 9 contains representative photomicrographs of calvarial cross-sections that clearly demonstrate an increased osteoid layer thickness in both ASARM groups (3.5-fold increase; $P < 0.001$) and the etidronate (2.35-fold increase; $P < 0.05$) relative to vehicle. This increase was statistically significant and confirms inhibition of mineralization by ASARM peptide groups as well as etidronate. This finding is also consistent with the data described in Figs. 6–8.

Discussion

The primary defects in X-linked hypophosphatemic rickets (HYP) and autosomal dominant hypophosphatemic rickets (ADHR) are loss of function mutations in the PHEX gene (a Zn metalloendopeptidase) and activating mutations in FGF23, respectively [23,29,70,73,91,92]. Oncogenic hypophosphatemic osteomalacia (OHO) is a rare tumor-induced disease and shares many pathophysiological features with HYP and ADHR. These include hypophosphatemia, defective/mineralization (osteomalacia/rickets), abnormal vitamin D metabolism, and elevated levels of FGF23 (full-length uncleaved) and MEPE [10,13,16,62,63,68,69,71,77,80,93]. Also, FGF23 levels in HYP are closely correlated with elevated MEPE expression [39].

The close correlation of FGF23 and MEPE levels in Hyp and the fact that intravenous injection of FGF23 or MEPE induces phosphaturia in rodents suggest that FGF23 may influence (directly or indirectly) MEPE expression or vice versa. Recently, we have demonstrated that MEPE, more specifically an 18-residue, carboxy-terminal MEPE peptide containing the ASARM motif (ASARM peptide), is a potent mineralization inhibitor when added to 2T3 osteoblasts in vitro [71]. Also, MEPE is a potent inhibitor of phosphate uptake in vivo and in vitro (bolus and infusion), and this is likely mediated directly by free MEPE–ASARM peptide [14,71]. Thus, this combination of findings suggests that MEPE, or more specifically the ASARM peptide, could be downstream of an FGF23 and/or phosphatonin extraosseous signaling pathway and play an important role in bone–renal mineral homeostasis.

A number of bone-dentin genes mapping to chromosome 4q (including MEPE) share many features and have been grouped into the SIBLING family (short integrin-binding ligand-interacting glycoproteins) [21,22,68,69,71]. Specifically, the SIBLINGs MEPE, DMP-1, DSPP, and OPN contain ASARM motif(s) or related phosphorylated peptides that are capable of inhibiting mineralization and/or phosphate uptake [28,44,64,68,69,71,76,83,90]. This is exemplified dramatically by an ancestral 'SIBLING-related' gene, statherin, which also maps to the same chromosome-4q SIBLING cluster region. Remarkably, statherin, a short 63-residue salivary protein, also contains an ASARM motif, and the statherin short ASARM peptide [DSSEE(K)] directly modulates the dynamics of tooth mineralization and is also thought to play a key role in the transport of phosphate and calcium in the parotid glands [44,64,76]. Moreover, the statherin ASARM peptide is directly responsible for preventing the ectopic precipitation of phosphate and calcium salts from supersaturated saliva. Thus, the evidence strongly supports the notion that this acidic, highly charged, aspartic acid/serine-enriched, phosphorylated motif plays a key role(s) in mineralization and perhaps phosphate transport when released as a small ASARM peptide [68].

In this regard, excess 'abnormal production' of MEPE ASARM peptide is likely responsible (wholly or in part) for the end-point mineralization defect and renal phosphate leak in HYP and/or OHO. This is because osteoblastic proteases and MEPE expression are both markedly elevated in HYP and OHO [2,3,13,17,26,27,32,33,39,40,68,69,77,80]. Moreover, the short 18-residue ASARM peptide is remarkably resistant to a vast number of proteases [68]. Thus, elevated MEPE and protease expression in defective HYP osteoblasts will likely result in a coordinate increase in protease-resistant ASARM peptide. In addition, and surprisingly for a Zn metalloendopeptidase, PHEX protects MEPE from proteolysis in vitro, and PHEX is also inhibited nonproteolytically by another important matrix protein, osteocalcin [6,27]. Therefore, absence of functional PHEX in HYP may compound ASARM peptide production by virtue of a loss of sequestration and thus loss of protease protection of MEPE by PHEX [68]. Specifically, our previous studies have confirmed that PHEX and a mutated (nonfunctional) carboxy-terminal PHEX fragment do not degrade MEPE but are both capable of protecting MEPE from cathepsin B proteolysis in vitro [27]. Cathepsin B is expressed and actively secreted by osteoblasts and could therefore act in concert with other proteases known to be elevated in HYP and degrade MEPE (NEP, ECL1/DINE, cathepsin D; [1,17,32,33]). The increased proteolytic degradation of overexpressed MEPE, in the absence of PHEX protection, likely results in the release of large quantities of protease-resistant MEPE–ASARM peptide in HYP [68,71].

Consistent with the HYP-ASARM protease model is the finding that specific protease inhibitors ameliorate the mineralization defect in HYP (in vitro) and also prevent the release of osteoblast-derived, phosphate inhibiting factors. Specifically, cathepsin D, neprilysin (NEP), and ECEL1/DINE proteases are markedly up-regulated in Hyp mice osteoblasts and bone marrow stromal cells (BMSC) [17,32,33], and there is a strong correlation between the inhibition of P(i) uptake by conditioned media (CM) from Hyp cells and elevated NEP-like activities. Other investigators have confirmed NEP mRNA and protein expression in mouse bone tissue including bone-forming cells, osteoblast precursors, preosteoblasts, osteoblasts, and osteocytes [74]. Further support for the HYP-ASARM model comes from findings that cathepsin D supplementation inhibits osteoblast cell mineralization, and an improvement of the Hyp mouse mineralization defect occurs on addition of pepsatin (a cathespin D inhibitor) [32,33]. Also, incubating Hyp osteoblasts with phosphoramidon (protease inhibitor) prevents the production of an osteoblast-secreted inhibitor of renal phosphate [P(i)] uptake [17,32,33] and is consistent with a protease inhibitor (phosphoramidon, pepstatin)-mediated reduction in free ASARM peptide in the Hyp osteoblast. This again is consistent with a prevention or reduction of proteolytic release of the protease-resistant osteoblastic MEPE–ASARM peptide (mineralization inhibitor).

Given the overlapping pathophysiology of HYP and OHO, of further interest is the finding that the renal phosphate inhibitory activity of conditioned media from OHO tumors cannot be inactivated by proteolytic digestion with trypsin, proteinase K, and/or papain [34,51,94]. However, these enzymes efficiently abolish the capacity of parathyroid (PTH) and parathyroid extracts to inhibit renal phosphate uptake in vitro [34]. Size ultrafiltration experiments also indicate that tumor phosphatonin-minhibin activity is due to small (<5 kDa) protease resistant molecules [11,34,35,51,56,57,94]. These findings are also consistent with the notion that the small proteolytically resistant ASARM peptide is a phosphatonin and/or minhibin [71]. Indeed, the uncharacterized, small molecular weight, protease-resistant, phosphaturic HPLC OHO tumor fractions described by Jonsson et al. 2001 [34] share very similar features (HPLC retention, etc.) to the synthetic, phosphorylated ASARM peptide described in this study and our previous study [71]. Of further significance is the finding that MEPE is highly expressed in all OHO tumors screened to date and is notably absent from nonphosphaturic tumors [13,69,77,80]. Moreover, DMP-1 is reported to be the second most highly expressed protein expressed in OHO tumors, and MEPE is the highest expressed [13,77,80,84]. Significantly, both SIBLINGs (MEPE and DMP-1) have carboxy-terminal ASARM motifs with a high degree of homology [68,69,71]. In one study, antibodies directed against the COOH-terminal region of DMP-1 (the ASARM motif region) were used to confirm a markedly elevated expression of OHO tumor-derived DMP-1 in three OHO cases studied [84]. Moreover, the same study showed a complete absence of DMP-1 protein expression in eleven “nonphosphaturic” soft tissue tumors including hemangiopericytomas. Similar results have been obtained with MEPE, and this strongly supports our current and previous experiments concerning the role of the ASARM peptide as renal phosphate inhibitor and mineralization inhibitor [67,68,71]. Also, other studies have reported that not all OHO tumors express FGF23 [13]. Thus, as indicated earlier, it is possible that FGF23 acts upstream of a signaling pathway that impacts on expression of matrix proteins like MEPE and/or DMP-1.

Although we have confirmed PHEX protection of MEPE in vitro in our previous studies, we did not determine whether the protection was due to a direct PHEX–MEPE interaction and/or indirect modification of protease activity [27]. The data presented in this study show for the first time that PHEX binds specifically to MEPE in a dose-dependent and Zn-dependent manner. Moreover, the carboxy-terminal ASARM motif region of full-length MEPE plays a key role in this interaction, and the Zn dependency of the interaction also implicates the PHEX Zn motif substrate-binding site [73] of nascent secPHEX. Since release of the ASARM peptide is critical for mineralization inhibition, binding of the ASARM motif region by the PHEX substrate site (Zn motif region) is consistent with a PHEX protease-protective role and also supports our recently proposed ASARM mineralization model [68,71]. Of further interest is our finding that the phosphorylated ASARM peptide (PO_4-ASARM peptide) is more effective at inhibiting PHEX–MEPE binding than the nonphosphorylated ASARM peptide (apparent K_{Dapp}’s of 15 and 35 uM, respectively). Interestingly, the Hyp mouse has an osteoblast casein kinase II defect that reportedly leads to abnormal phosphorylation of another SIBLING family member, osteopontin [66,99]. Further experiments are required to confirm whether this Hyp osteoblast defect (casein kinase II, osteoblast-ectokinase) has relevance to the ASARM peptide, MEPE–PHEX binding, and/or Hyp pathophysiology.

The key residue characteristics of the SIBLING protein (MEPE, DMP-1, OPN, and DSPP) and salivary statherin ASARM peptides are the enriched aspartic acid (D), serine (S), glutamic acid (E) residues, and phosphoserines. Thus, the peptides are acidic, highly charged, with low pI’s, and are extraordinarily resistant to a wide range of proteases. Indeed, they all have physicochemical similarities to bisphosphonates, phosphonoformic acid (PFA), and phosphonoacetic acid (PAA). Also, they share biological properties in vivo and in vitro

with bisphosphonates, PFA, and PAA in that they all inhibit mineralization and interfere with renal phosphate handling and vitamin D metabolism [7,36,41–43,46,47,55,81,82,85,87,88]. Our studies confirm for the first time that the MEPE ASARM peptide inhibits mineralization in vivo, and this is consistent with previous in vitro results and in vivo salivary data with the statherin ASARM peptide. Moreover, this is consistent with previous studies that demonstrated marked phosphate uptake and mineralization inhibition activity associated with HYP osteoblasts, Hyp osteoblast-conditioned media, and Hyp serum compared to normal sibling controls [18–20,35,48,49,58,78,95,96]. Also consistent is the finding that the MEPE null-mutant mouse has a phenotype that not only presents with increased bone mass, increased numbers and thickness of trabeculae, and cortical bone mass, but also has an accelerated osteoblast mineralization rate in vitro plus an increased mineralization apposition rate in vivo [25].

Elegant studies have confirmed that PHEX can cleave small, synthetic, quenched fluorogenic peptides of the ASARM motif (QF-ASARMp) [12]. Cleavage does not result in degradation of the ASARM motif but results in cleavage of specific residues that reside N-terminal to aspartic acid (D). Specifically, of the residues investigated using small QF peptides derived from FGF23 and MEPE, cleavages between a serine (S) and D residue (K_{cat}/K_m = 80 to 125 $mM^{-1} \cdot s^{-1}$) and between D and D residues (K_{cat}/K_m = 80 to 125 $mM^{-1} \cdot s^{-1}$= 67 to 100) were found to be catalyzed with the highest activity. All other residues within diverse peptide sequence formats were cleaved N-terminal to D residues (*Y*-**D**; *E*-**D**; *R*-**D**; *L*-**D**; and *N*-**D**) at very low efficiencies (K_{cat}/K_m = 0.8 to 15 $mM^{-1} \cdot s^{-1}$). One exception was cleavage between M and D residues which had intermediate catalytic efficiency (K_{cat}/K_m = 47 $mM^{-1} \cdot s^{-1}$). Thus, from these studies, we would predict that PHEX cleavage of the ASARM motif region from a mouse, rat, and human ASARM peptide would generate the following peptides (the hyphen between residues indicates potential cleavage site): (1) mouse RQR-DSSESSSSGSSSESHGD; (2) rat RQR-DSSESSSSGSSSESSGD; (3) human RR-D-DSSESS-DSGSSSESDGD. In all cases, the active ASARM motif residues would not be affected and, with the human ASARM peptide, would result (potentially) in the release of a small peptide sequence DSSESS that is similar to the biologically active statherin ASARM peptide (DSSEE{K}) [44,64,76]. This short statherin sequence (DSSEE{K}) is known to be a powerful inhibitor of hydroxyapatite formation and plays a major biological role in preventing ectopic precipitation of calcium phosphate from supersaturated saliva, stabilization of tooth enamel, and for the inhibition of formation of mineral accretions on tooth surfaces [64]. Also, the remaining human sequence (DSGSSSESDGD) would also predictably have the same ASARM motif characteristics. In both the mouse and rat, the active ASARM peptide molecule would essentially remain intact following exposure to PHEX. A further important consideration is that PHEX does not appear to cleave full-length MEPE or full-length FGF23 [12,27,39,40] and is therefore thought to require smaller oligopeptide substrates [12]. We would propose that, although the full-length MEPE molecule binds to PHEX via the ASARM motif, the molecular topography of the full-length protein–protein interactions may not be conducive for cleavage. In this regard, the proteolytic activity of PHEX on oligopeptide substrates of diverse sizes needs to be clarified.

These observations extend our recent findings of a nonproteolytic PHEX–MEPE interaction [27] by demonstrating a direct Zn-dependent interaction involving the MEPE ASARM motif. The data are also consistent with recent observations of PHEX nonproteolytic interactions with another matrix protein osteocalcin [6]. Similarly, our recently published in vitro observations of ASARM peptide mineralization inhibition have now been extended to in vivo confirmation of minhibin activity [68,71] and also are in agreement with in vitro findings of inhibition of mineralization and/or hydroxyapatite formation by ASARM peptides derived from statherin, osteopontin, MEPE, and potentially other related SIBLING

proteins [28,44,64,68,69,71,76, 83,90]. In addition, our observations are consistent with the pathophysiology of HYP and the proposed HYP-ASARM model [68,71]. Specifically, loss of PHEX function is proposed to directly result in defective mineralization by virtue of a loss of MEPE sequestration by PHEX, a concomitant increase in extracellular matrix protease degradation of MEPE, and subsequent release of protease resistant ASARM peptide(s) (minhibin). This pathophysiology is exacerbated by the well-documented increase in osteoblastic proteases and increased expression of MEPE in HYP [2,3,17,27,32,33,39,40]. Moreover, M13 Zn metal-loendopeptidases like KELL antigen form heterodimers (KELL and XK protein), and three MEPE SIBLING family members (OPN, DMP-1, and BSP) form protein–protein (nonproteolytic) interactions with matrix metalloproteins (MMPs) [21,37,65,86]. In SIBLING–MMP, nonproteolytic protein interactions appear to play key roles in modulating the biological activity of these proteases [21]. Indeed, cartilage abnormalities and defective mineralization have recently been associated with abnormal PHEX expression and with altered matrix protein and matrix metalloproteinase-9 (MMP9) localization in Hyp mice [50].

Although the PHEX protection ASARM model is consistent with HYP pathophysiology, we cannot exclude the possibility that a MEPE–PHEX nonproteolytic interaction may be required to activate PHEX activity as has been reported for specific MMPs (matrix metalloproteinases) and three related SIBLING proteins (OPN, DMP-1, BSP) [21]. In this regard, excess free phosphorylated ASARM peptide may also interfere or modify PHEX activity as well as inhibiting mineralization and renal phosphate handling. Of further note is the finding that PPi and phosphate can act as inhibitors of PHEX-mediated proteolysis of parathyroid hormone-related peptide 107–139 (PTHrp107–139), the only known ‘naturally’ occurring substrate of PHEX [6]. Interestingly, PTHrp107–139, unlike PHEX, is absent in bony fish (teleosts) and is not thought to be a physiological substrate [5].

Clearly, more work needs to be done to confirm a number of molecular aspects. Although other ASARM peptides like the salivary statherin ASARM peptide have been investigated biologically, the relative levels of MEPE ASARM peptide in Hyp, OHO, and normal extracellular matrix and serum need to be accurately determined. Elevated levels in these hypophosphatemic diseases (Hyp, OHO, and perhaps ADHR) would be strongly supportive for a role in the mineralization/phosphate defect, particularly if the levels are commensurate with the amounts required to inhibit mineralization and/or renal phosphate handling in vivo. Also, the potential contribution of other free extracellular matrix ASARM peptide sources must be assessed. Moreover, the role of other signaling molecules implicated in mineralization and hypophosphatemic disorders (FGF23 and FRP4) and their impact on expression of PHEX, MEPE, extracellular matrix ASARM peptide(s), and/or other matrix proteins (DMP-1, vitronectin, BSP, etc.) need to be thoroughly investigated. Finally, the biological nature of PHEX interactions with matrix proteins such as MEPE and osteocalcin as well as phosphate and PPi also requires further investigation. This needs to be done within the framework of mineralization and renal phosphate homeostasis across a bone–renal axis. In this context, our data and work from others suggest that PHEX in bone and also in brain may be multifunctional and act as either a direct matrix protein–ligand and/or protease and/or require activation by protein–protein interaction with other matrix proteins. Fig. 10 presents a simplified scheme of the ASARM model and the proposed role of MEPE, PHEX, FGF23, and ASARM peptide in mineralization and phosphate homeostasis.

In summary, we would propose that given the vast tissue resource of bone and teeth and thus associated extracellular matrix sibling proteins, the control of a free mineralization inhibitor (minhibin) ASARM peptide is critical for healthy mineralization. Moreover, PHEX may play a key role in bone and teeth by regulating this process in an unexpected and novel way. More precisely, our data suggest that this would involve the temporal and reversible

protease protection of MEPE and consequential prevention of uncontrolled release of protease-resistant ASARM peptide(s).

Acknowledgments

The authors would like to acknowledge the very kind gift of pure secPHEX by Dr. Philippe Crine (Department of Biochemistry, University of Montréal and BIOMEP) and Dr. Guy Boileau (Department of Biochemistry, University of Montréal). We also acknowledge the generous financial support and awards to PSNR: Children's Cancer Research Center (CCRC) of the University of Texas Health Science Center at San Antonio (UTHSCSA), National Institutes of Health grant 1R03DE015900-01 (National Institute of Dental and Craniofacial Research), and NIH grant RO-1 AR51598-01 (National Institute of Arthritis and Musculoskeletal Skin Diseases).

References

1. Aisa MC, Beccari T, Costanzi E, Maggio D. Cathepsin B in osteoblasts. Biochim Biophys Acta. 2003; 1621:149–159. [PubMed: 12726991]
2. Argiro L, Desbarats M, Glorieux FH, Ecarot B. Mepe, the gene encoding a tumor-secreted protein in oncogenic hypophosphatemic osteomalacia, is expressed in bone. Genomics. 2001; 74:342–351. [PubMed: 11414762]
3. Bai X, Miao D, Panda D, Grady S, McKee MD, Goltzman D, et al. Partial rescue of the Hyp phenotype by osteoblast-targeted PHEX (phosphate-regulating gene with homologies to endopeptidases on the X chromosome) expression. Mol Endocrinol. 2002; 16:2913–2925. [PubMed: 12456809]
4. Benet-Pages A, Lorenz-Depiereux B, Zischka H, White KE, Econs TM, Strom TM. FGF23 is processed by proprotein convertases but not by PHEX. Bone. 2004; 35:455–462. [PubMed: 15268897]
5. Bianchetti L, Oudet C, Poch O. M13 endopeptidases: new conserved motifs correlated with structure, and simultaneous phylogenetic occurrence of PHEX and the bony fish. Proteins. 2002; 47:481–488. [PubMed: 12001226]
6. Boileau G, Tenenhouse HS, Desgroseillers L, Crine P. Characterization of PHEX endopeptidase catalytic activity: identification of parathyroid-hormone-related peptide 107–139 as a substrate and osteocalcin, PPi and phosphate as inhibitors. Biochem J. 2001; 355:707–713. [PubMed: 11311133]
7. Bonjour JP, Trechsel U, Fleisch H, Schenk R, DeLuca HF, Baxter LA. Action of 1,25-dihydroxyvitamin D3 and a diphosphonate on calcium metabolism in rats. Am J Physiol. 1975; 229:402–408. [PubMed: 808969]
8. Boskey AL. Osteopontin and related phosphorylated sialoproteins: effects on mineralization. Ann N Y Acad Sci. 1995; 760:249–256. [PubMed: 7785899]
9. Boskey AL, Spevak L, Paschalis E, Doty SB, McKee MD. Osteopontin deficiency increases mineral content and mineral crystallinity in mouse bone. Calcif Tissue Int. 2002; 71:145–154. [PubMed: 12073157]
10. Brame LA, White KE, Econs MJ. Renal phosphate wasting disorders: clinical features and pathogenesis. Semin Nephrol. 2004; 24:39–47. [PubMed: 14730508]
11. Cai Q, Hodgson SF, Kao PC, Lennon VA, KLee GG, Zinsmiester AR, et al. Brief report: inhibition of renal phosphate transport by a tumor product in a patient with oncogenic osteomalacia. N Engl J Med. 1994; 330:1645–1649. [PubMed: 8177270]
12. Campos M, Couture C, Hirata IY, Juliano MA, Loisel TP, Crine P, et al. Human recombinant endopeptidase PHEX has a strict S1′ specificity for acidic residues and cleaves peptides derived from fibroblast growth factor-23 and matrix extracellular phosphoglycoprotein. Biochem J. 2003; 373:271–279. [PubMed: 12678920]
13. De Beur SM, Finnegan RB, Vassiliadis J, Cook B, Barberio D, Estes S, et al. Tumors associated with oncogenic osteomalacia express genes important in bone and mineral metabolism. J Bone Miner Res. 2002; 17:1102–1110. [PubMed: 12054166]
14. Dobbie H, Shirley DG, Faria NJ, Rowe PSN, Slater JM, Unwin RJ. Infusion of the bone-derived protein MEPE causes phosphaturia in rats (abstract). J Am Soc Nephrol. 2003; 14:468A.

15. Donath K, Breuner G. A method for the study of undecalcified bones and teeth with attached soft tissues. The Sage-Schliff (sawing and grinding) technique. J Oral Pathol. 1982; 11:318–326. [PubMed: 6809919]
16. Drezner MK. Tumor-induced osteomalacia. Rev Endocr Metab Disord. 2001; 2:175–186. [PubMed: 11705323]
17. Dubois SG, Ruchon AF, Delalandre A, Boileau G, Lajeunesse D. Role of abnormal neutral endopeptidase-like activities in Hyp mouse bone cells in renal phosphate transport. Am J Physiol: Cell Physiol. 2002; 283:C1414. [PubMed: 12372802]
18. Ecarot B, Glorieux FH, Desbarats M, Travers R, Labelle L. Defective bone formation by Hyp mouse bone cells transplanted into normal mice: evidence in favor of an intrinsic osteoblast defect. J Bone Miner Res. 1992; 7:215–220. [PubMed: 1315116]
19. Ecarot B, Glorieux FH, Desbarats M, Travers R, Labelle L. Effect of 1,25-dihydroxyvitamin D3 treatment on bone formation by transplanted cells from normal and X-linked hypophosphatemic mice. J Bone Miner Res. 1995; 10:424–431. [PubMed: 7785464]
20. Ecarot FH, Glorieux FH, Desbarats M, Travers R, Labelle L. Effect of dietary phosphate deprivation and supplementation of recipient mice on bone formation by transplanted cells from normal and X-linked hypophosphataemic mice. J Bone Miner Res. 1992; 7(5):523–530. [PubMed: 1319665]
21. Fedarko NS, Jain A, Karadag A, Fisher LW. Three small integrin-binding ligand *N*-linked glycoproteins (SIBLINGs) bind and activate specific matrix metalloproteinases. FASEB J. 2004; 18:734–736. [PubMed: 14766790]
22. Fisher LW, Torchia DA, Fohr B, Young MF, Fedarko NS. Flexible structures of SIBLING proteins, bone sialoprotein, and osteopontin. Biochem Biophys Res Commun. 2001; 280:460–465. [PubMed: 11162539]
23. Francis F, Strom TM, Hennig S, Boeddrich A, Lorenz B, Brandau O, et al. Genomic organisation of the human PEX gene mutated in X-linked dominant hypophosphataemic rickets. Genet Res. 1997; 7(6):573–585.
24. Garrett IR, Chen D, Gutierrez G, Zhao M, Escobedo A, Rossini G, et al. Selective inhibitors of the osteoblast proteasome stimulate bone formation in vivo and in vitro. J Clin Invest. 2003; 111:1771–1782. [PubMed: 12782679]
25. Gowen LC, Petersen DN, Mansolf AL, Qi H, Stock JL, Tkalcevic GT, et al. Targeted disruption of the osteoblast/osteocyte factor 45 gene (OF45) results in increased bone formation and bone mass. J Biol Chem. 2003; 278:1998–2007. [PubMed: 12421822]
26. Guo R, Liu S, Spurney RF, Quarles LD. Analysis of recombinant Phex: an endopeptidase in search of a substrate. Am J Physiol: Endocrinol Metab. 2001; 281:E837–E847. [PubMed: 11551862]
27. Guo R, Rowe PS, Liu S, Simpson LG, Xiao ZS, Quarles LD. Inhibition of MEPE cleavage by Phex. Biochem Biophys Res Commun. 2002; 297:38–45. [PubMed: 12220505]
28. Hoyer JR, Asplin JR, Otvos L. Phosphorylated osteopontin peptides suppress crystallization by inhibiting the growth of calcium oxalate crystals. Kidney Int. 2001; 60:77–82. [PubMed: 11422738]
29. Francis F, Hennig S, Korn B, Reinhardt R, de Jong D, et al. HYP-consortium. A gene (PEX) with homologies to endopeptidases is mutated in patients with X-linked hypophosphatemic rickets. The HYP Consortium. Nat Genet. 1995; 11:130–136. [PubMed: 7550339]
30. Jain A, Fedarko NS, Collins MT, Gelman R, Ankrom MA, Tayback M, et al. Serum levels of matrix extracellular phosphoglycoprotein (MEPE) in normal humans correlate with serum phosphorus, parathyroid hormone and bone mineral density. J Clin Endocrinol Metab. 2004; 89:4158–4161. [PubMed: 15292364]
31. Jan de Beur SM, Levine MA. Molecular pathogenesis of hypophosphatemic rickets. J Clin Endocrinol Metab. 2002; 87:2467–2473. [PubMed: 12050201]
32. Jo OD, Shih R, Sun A, Pham P, Yanagawa J, Yanagawa N. Cathepsin D (Cat D) and bone defect in hypophosphatemic (Hyp) mice (abstract). J Am Soc Nephrol. 2000; 11:408A.
33. Jo OD, Yang F, Kuizon B, Shih HM, Yanagawa N. Increased apoptosis in Hyp mouse bone. Potential role of cathepsin D (Abstract). J Am Soc Nephrol. 2001; 12(A3881):743A.

34. Jonsson KB, Mannstadt M, Miyauchi A, Yang IM, Stein G, Ljunggren O, et al. Extracts from tumors causing oncogenic osteomalacia inhibit phosphate uptake in opossum kidney cells. J Endocrinol. 2001; 169:613–620. [PubMed: 11375132]
35. Lajeunesse D, Meyer RA Jr, Hamel L. Direct demonstration of a humorally-mediated inhibition of renal phosphate transport in the Hyp mouse. Kidney Int. 1996; 50:1531–1538. [PubMed: 8914019]
36. Lawson-Matthew PJ, Guilland-Cumming DF, Yates AJ, Russell RG, Kanis JA. Contrasting effects of intravenous and oral etidronate on vitamin D metabolism in man. Clin Sci (Lond). 1988; 74:101–106. [PubMed: 3123117]
37. Lee S, Russo D, Redman CM. The Kell blood group system: Kell and XK membrane proteins. Semin Hematol. 2000; 37:113–121. [PubMed: 10791880]
38. Lemire I, Lazure C, Crine P, Boileau G. Secretion of a type II integral membrane protein induced by mutation of the transmembrane segment. Biochem J. 1997; 322:335–342. [PubMed: 9078281]
39. Liu S, Guo R, Simpson LG, Xiao ZS, Burnham CE, Quarles LD. Regulation of FGF23 expression but not degradation by Phex. J Biol Chem. 2003; 278:37419–37426. [PubMed: 12874285]
40. Liu S, Guo R, Xiao G, Quarles LD. Regulation of FGF23 expression but not metabolism by Phex (abstract). J Bone Miner Res. 2003; 18(Suppl. 2):S50.
41. Loghman-Adham M, Dousa TP. Dual action of phosphonoformic acid on Na(+)-phosphate cotransport in opossum kidney cells. Am J Physiol. 1992; 263:F301–F310. [PubMed: 1380774]
42. Loghman-Adham M, Szczepanska-Konkel M, Dousa TP. Phosphate transport in brush border membranes from uremic rats. Response to phosphonoformic acid. J Am Soc Nephrol. 1992; 3:1253–1259. [PubMed: 1477321]
43. Loghman-Adham M, Szczepanska-Konkel M, Yusufi AN, Van Scoy M, Dousa TP. Inhibition of Na^+-Pi cotransporter in small gut brush border by phosphonocarboxylic acids. Am J Physiol. 1987; 252:G244–G249. [PubMed: 2950771]
44. Long JR, Dindot JL, Zebroski H, Kiihne S, Clark RH, Campbell AA, et al. A peptide that inhibits hydroxyapatite growth is in an extended conformation on the crystal surface. Proc Natl Acad Sci U S A. 1998; 95:12083–12087. [PubMed: 9770443]
45. MacDougall M, Simmons D, Gu TT, Dong J. MEPE/OF45, a new dentin/bone matrix protein and candidate gene for dentin diseases mapping to chromosome 4q21. Connect Tissue Res. 2002; 43:320–330. [PubMed: 12489176]
46. McCloskey EV, Yates AJ, Beneton MN, Galloway J, Harris S, Kanis JA. Comparative effects of intravenous diphosphonates on calcium and skeletal metabolism in man. Bone. 1987; 8:S35–S41. [PubMed: 2825741]
47. McCloskey EV, Yates AJ, Gray RE, Hamdy NA, Galloway J, Kanis JA. Diphosphonates and phosphate homeostasis in man. Clin Sci (Lond). 1988; 74:607–612. [PubMed: 3396298]
48. Meyer RA Jr, Meyer MA, Gray RW. Parabiosis suggests a humoral factor is involved in X-linked hypophosphataemia in mice. J Bone Miner Res. 1989; 4(4):493–500. [PubMed: 2816498]
49. Meyer RA Jr, Tenenhouse HS, Meyer MA, Klugerman AH. The renal phosphate transport defect in normal mice parabiosed to X-linked hypophosphataemic mice persists after parathyroidectomy. J Bone Miner Res. 1989; 4(4):523–532. [PubMed: 2816501]
50. Miao D, Bai X, Panda D, Karaplis AC, Goltzman D, McKee MD. Cartilage abnormalities are associated with abnormal Phex expression and with altered matrix protein and MMP-9 localization in Hyp mice. Bone. 2004; 34:638–647. [PubMed: 15050894]
51. Miyauchi A, Fukase M, Tsutsumi M, Fujita T. Hemangiopericytoma induced osteomalacia: tumour transplantation in nude mice causes hypophosphataemia and tumour extracts inhibit renal 25-hydroxyvitamin D α1-hydroxylase activity. J Clin Endocrinol Metab. 1988; 67(1):46–53. [PubMed: 2837500]
52. Morgan JR, Prasad K, Hao W, Augustine GJ, Lafer EM. A conserved clathrin assembly motif essential for synaptic vesicle endocytosis. J Neurosci. 2000; 20:8667–8676. [PubMed: 11102472]
53. Morgan JR, Prasad K, Jin S, Augustine GJ, Lafer EM. Eps15 homology domain-NPF motif interactions regulate clathrin coat assembly during synaptic vesicle recycling. J Biol Chem. 2003; 278:33583–33592. [PubMed: 12807910]

54. Morgan JR, Prasad K, Jin S, Augustine GJ, Lafer EM. Uncoating of clathrin-coated vesicles in presynaptic terminals: roles for Hsc70 and auxilin. Neuron. 2001; 32:289–300. [PubMed: 11683998]
55. Muhlbauer RC, Bonjour JP, Fleisch H. Tubular handling of phosphate along the nephron of thyroparathyroidectomized rats injected with ethane-1-hydroxy-1,1-diphosphonate. Clin Sci (Lond). 1981; 60:171–177. [PubMed: 6786814]
56. Nelson AE, Hogan JJ, Holm IA, Robinson BG, Mason RS. Phosphate wasting in oncogenic osteomalacia: PHEX is normal and the tumor-derived factor has unique properties. Bone. 2001; 28:430–439. [PubMed: 11336925]
57. Nelson AE, Namkung HJ, Patava J, Wilkinson MR, Chang AM, Reddel RR, et al. Characteristics of tumor cell bioactivity in oncogenic osteomalacia. Mol Cell Endocrinol. 1996; 124:17–23. [PubMed: 9027320]
58. Nesbitt T, Fujiwara I, Thomas R, Xiao ZS, Quarles LD, Drezner MK. Coordinated maturational regulation of PHEX and renal phosphate transport inhibitory activity: evidence for the pathophysiological role of PHEX in X-linked hypophosphatemia. J Bone Miner Res. 1999; 14:2027–2035. [PubMed: 10620061]
59. Okano T, Tsugawa N, Hirami C, Kato S. Functional properties of cultured normal and vitamin D receptor knockout mice calvarial osteoblasts (abstract). J Bone Miner Res. 2003; 18(Suppl. 2):S141.
60. Papagerakis S, Rowe PSN, MacDougall M. MEPE expression pattern in craniofacial mineralized tissues. J Dent Res. 2004 [submitted for publication].
61. Petersen DN, Tkalcevic GT, Mansolf AL, Rivera-Gonzalez R, Brown TA. Identification of osteoblast/osteocyte factor 45 (OF45), a bone-specific cDNA encoding an RGD-containing protein that is highly expressed in osteoblasts and osteocytes. J Biol Chem. 2000; 275:36172–36180. [PubMed: 10967096]
62. Quarles LD. FGF23, PHEX, and MEPE regulation of phosphate homeostasis and skeletal mineralization. Am J Physiol: Endocrinol Metab. 2003; 285:E1. [PubMed: 12791601]
63. Quarles LD, Drezner MK. Pathophysiology of X-linked hypophosphatemia, tumor-induced osteomalacia, and autosomal dominant hypophosphatemia: a perPHEXing problem. J Clin Endocrinol Metab. 2001; 86:494–496. [PubMed: 11157997]
64. Raj PA, Johnsson M, Levine MJ, Nancollas GH. Salivary statherin. Dependence on sequence, charge, hydrogen bonding potency, and helical conformation for adsorption to hydroxyapatite and inhibition of mineralization. J Biol Chem. 1992; 267:5968–5976. [PubMed: 1313424]
65. Rawlings, ND.; Barrett, AJ. Evolutionary families of metallopeptidases. In: Barrett, AJ., editor. Methods Enzymol. Vol. vol. 248. New York: Academic Press; 1995. p. 183-228.
66. Rifas L, Cheng S, Halstead LR, Gupta A, Hruska KA, Avioli LV. Skeletal casein kinase activity defect in the HYP mouse. Calcif Tissue Int. 1997; 61:256–259. [PubMed: 9262518]
67. Rowe PS. The molecular background to hypophosphataemic rickets. Arch Dis Child. 2000; 83:192–194. [PubMed: 10952628]
68. Rowe PSN. The wrickkened-pathways of FGF23, MEPE and PHEX. Crit Rev Oral Biol Med. 2004; 15:264–281. [PubMed: 15470265]
69. Rowe PSN, de Zoysa P, Dong R, Wang H, White K, Econs M, et al. MEPE, a new gene expressed in bone-marrow and tumours causing osteomalacia. Genomics. 2000; 67(1):54–68. [PubMed: 10945470]
70. Rowe PSN, Goulding JN, Francis F, Oudet C, Econs MJ, Hanauer A, et al. The gene for X-linked hypophosphataemic rickets maps to a 200–300 kb region in Xp22.1, and is located on a single YAC containing a putative vitamin D response element (VDRE). Hum Genet. 1996; 97:345–352. [PubMed: 8786079]
71. Rowe PSN, Kumagai Y, Gutierrez G, Garrett IR, Blacher R, Rosen D, et al. MEPE has the properties of an osteoblastic phosphatonin and minhibin. Bone. 2004; 34:303–319. [PubMed: 14962809]
72. Rowe PSN, Ong A, Cockerill F, Goulding J, Hewison M. Candidate 56 and 58 kDa protein(s) responsible for mediating the renal defects in oncogenic hypophosphataemic osteomalacia. Bone. 1996; 18(2):159–169. [PubMed: 8833210]

73. Rowe PSN, Oudet C, Francis F, Sinding C, Pannetier S, Econs MJ, et al. Distribution of mutations in the PEX gene in families with X-linked hypophosphataemic rickets (HYP). Hum Mol Genet. 1997; 6:539–549. [PubMed: 9097956]
74. Ruchon AF, Marcinkiewicz M, Ellefsen K, Basak A, Aubin J, Crine P, et al. Cellular localization of neprilysin in mouse bone tissue and putative role in hydrolysis of osteogenic peptides. J Bone Miner Res. 2000; 15:1266–1274. [PubMed: 10893675]
75. Sanderson C, Bachus KN. Staining technique to differentiate mineralized and demineralized bone in ground sections. J Histotechnol. 1997; 20:119–122.
76. Schwartz SS, Hay DI, Schluckebier SK. Inhibition of calcium phosphate precipitation by human salivary statherin: structure–activity relationships. Calcif Tissue Int. 1992; 50:511–517. [PubMed: 1525706]
77. Seufert J, Ebert K, Muller J, Eulert J, Hendrich C, Werner E, et al. Octreotide therapy for tumor-induced osteomalacia. N Engl J Med. 2001; 345:1883–1888. [PubMed: 11756579]
78. Shih NR, Jo OD, Yanagawa N. Effects of PHEX antisense in human osteoblast cells. J Am Soc Nephrol. 2002; 13:394–399. [PubMed: 11805167]
79. Shimada T, Hasegawa H, Yamazaki Y, Muto T, Hino R, Takeuchi Y, et al. FGF-23 is a potent regulator of vitamin D metabolism and phosphate homeostasis. J Bone Miner Res. 2004; 19:429–435. [PubMed: 15040831]
80. Shimada T, Mizutani S, Muto T, Yoneya T, Hino R, Takeda S, et al. Cloning and characterization of FGF23 as a causative factor of tumor-induced osteomalacia. Proc Natl Acad Sci U S A. 2001; 98:6500–6505. [PubMed: 11344269]
81. Stoll R, Fleisch H, Bonjour JP. Effect of diphosphonate treatment on phosphate transport by renal brush border vesicles. Am J Physiol. 1980; 239:F13–F16. [PubMed: 6772037]
82. Szczepanska-Konkel M, Yusufi ANK, VanScoy M, Webster SK, Dousa TP. Phosphonocarboxylic acids as specific inhibitors of Na^+-dependent transport of phosphate across renal brush border membrane. J Biol Chem. 1986; 261:6375–6383. [PubMed: 3009455]
83. Tartaix PH, Doulaverakis M, George A, Fisher LW, Butler WT, Qin C, et al. Dentin matrix protein-1: in vitro effects on hydroxyapatite formation provide insights into in vivo functions. J Biol Chem. 2004; 279:18115–18120. [PubMed: 14769788]
84. Toyosawa S, Tomita Y, Kishino M, Hashimoto J, Ueda T, Tsujimura T, et al. Expression of dentin matrix protein 1 in tumors causing oncogenic osteomalacia. Mod Pathol. 2004; 17:573–578. [PubMed: 15001995]
85. Trechsel U, Schenk R, Bonjour JP, Russell RG, Fleisch H. Relation between bone mineralization, Ca absorption, and plasma Ca in phosphonate-treated rats. Am J Physiol. 1977; 232:E298–E305. [PubMed: 402823]
86. Turner AJ, Isaac RE, Coates D. The neprilysin (NEP) family of zinc metalloendopeptidases: genomics and function. BioEssays. 2001; 23:261–269. [PubMed: 11223883]
87. VanScoy M, Loghman-Adham M, Onsgard M, Szczepanska-Konkel S, Homma S, Knox FG, et al. Mechanism of phosphaturia elicited by administration of phosphonoformate in vivo. Am J Physiol. 1988; 255:F984–F994. [PubMed: 2847555]
88. Walton RJ, Russell RG, Smith R. Changes in the renal and extrarenal handling of phosphate induced by disodium etidronate (EHDP) in man. Clin Sci Mol Med. 1975; 49:45–56. [PubMed: 807449]
89. Weber TJ, Liu S, Indridason OS, Quarles LD. Serum FGF23 levels in normal and disordered phosphorus homeostasis. J Bone Miner Res. 2003; 18:1227–1233. [PubMed: 12854832]
90. Wesson JA, Johnson RJ, Mazzali M, Beshensky AM, Stietz S, Giachelli C, et al. Osteopontin is a critical inhibitor of calcium oxalate crystal formation and retention in renal tubules. J Am Soc Nephrol. 2003; 14:139–147. [PubMed: 12506146]
91. White KE, Carn G, Lorenz-Depiereux B, Benet-Pages A, Strom TM, Econs MJ. Autosomal-dominant hypophosphatemic rickets (ADHR) mutations stabilize FGF-23. Kidney Int. 2001; 60:2079–2086. [PubMed: 11737582]
92. White KE, Evans WE, O'Riordan JLH, Speer MC, Econs MJ, Lorenz-Depiereux B, et al. Autosomal dominant hypophosphataemic rickets is associated with mutations in FGF23. Nat Genet. 2000; 26:345–348. [PubMed: 11062477]

93. White KE, Jonsson KB, Carn G, Hampson G, Spector TD, Mannstadt M, et al. The autosomal dominant hypophosphatemic rickets (ADHR) gene is a secreted polypeptide overexpressed by tumors that cause phosphate wasting. J Clin Endocrinol Metab. 2001; 86:497–500. [PubMed: 11157998]

94. Wilkins GE, Granleese S, Hegele RG, Holden J, Anderson GP, Bondy GP. Oncogenic osteomalacia: evidence for a humoral phosphaturic factor. J Clin Endocrinol Metab. 1995; 80:1628–1634. [PubMed: 7745010]

95. Xiao ZS, Crenshaw M, Guo R, Nesbitt T, Drezner MK, Quarles LD. Intrinsic mineralization defect in Hyp mouse osteoblasts. Am J Physiol. 1998; 275:E700–E708. [PubMed: 9755091]

96. Yamamoto T, Ecarot B, Glorieux FH. Abnormal response of osteoblasts from Hyp mice to 1,25-dihydroxyvitamin D3. Bone. 1992; 13:209–215. [PubMed: 1322149]

97. Yamashita T, Yoshioka M, Itoh N. Identification of a novel fibroblast growth factor, FGF-23, preferentially expressed in the ventrolateral thalamic nucleus of the brain. Biochem Biophys Res Commun. 2000; 277:494–498. [PubMed: 11032749]

98. Zhang GX, Mizuno M, Tsuji K, Tamura M. Regulation of mRNA expression of matrix extracellular phosphoglycoprotein (MEPE)/osteoblast/osteocyte factor 45 (OF45) by fibroblast growth factor 2 in cultures of rat bone marrow-derived osteoblastic cells. Endocrine. 2004; 24:15–24. [PubMed: 15249699]

99. Zhu X, Luo C, Ferrier JM, Sodek J. Evidence of ectokinase-mediated phosphorylation of osteopontin and bone sialoprotein by osteoblasts during bone formation in vitro. Biochem J. 1997; 323:637–643. [PubMed: 9169595]

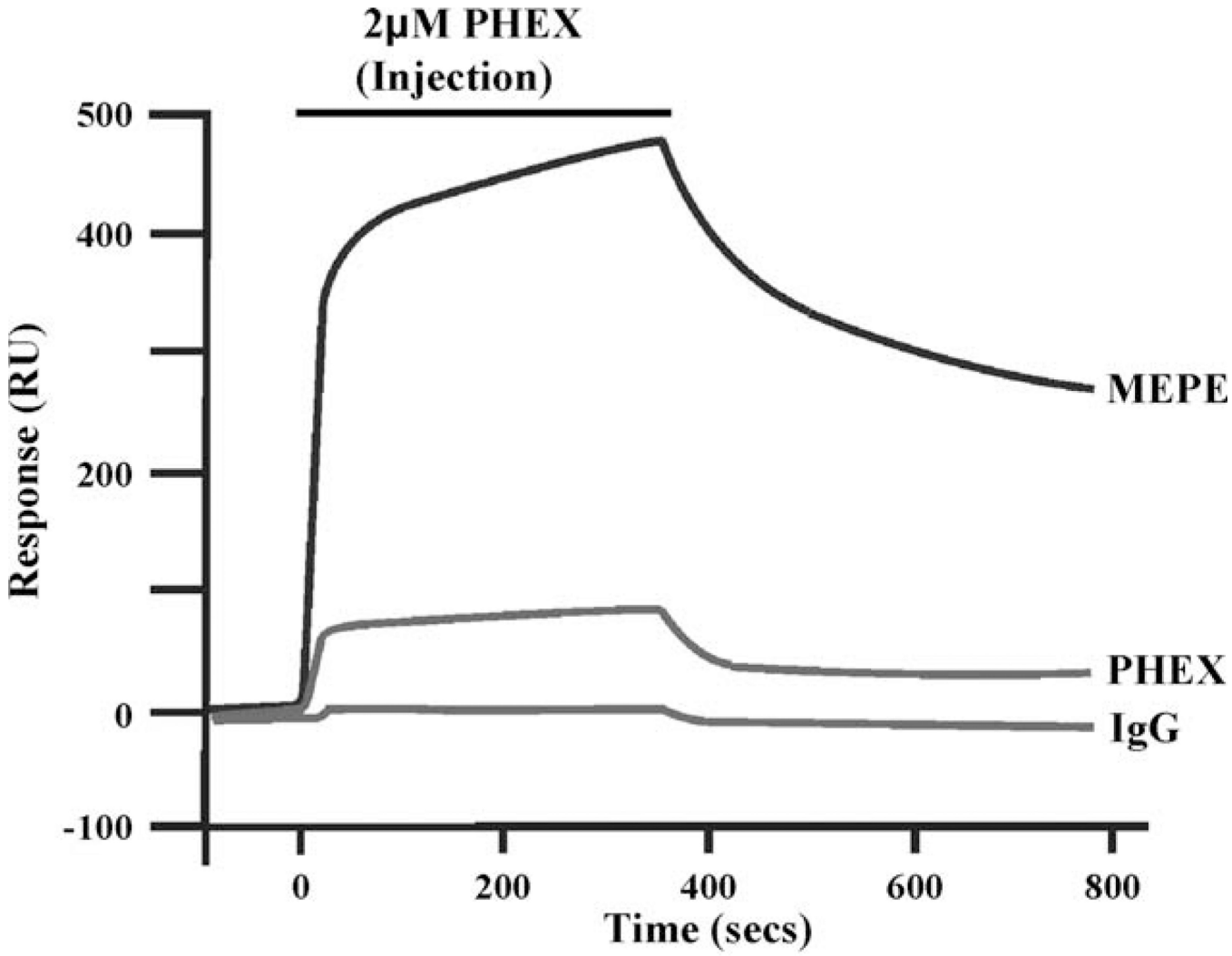

Fig. 1.

Biacore sensorgram of chip-immobilized MEPE, PHEX, and IgG ligands against secPHEX analyte (mobile phase). PHEX binds to MEPE, and the binding requires $ZnCl_2$ (2 mM)-supplemented buffer (HBS-P-Zn). Specifically, no PHEX–MEPE binding was observed with buffer lacking $ZnCl_2$ and concentrations of PHEX analyte up to 10 uM (data not shown). Ligands (MEPE, PHEX, and IgG) were each coupled to a Biacore CM-5 chip at 3500 RU and 2 uM secPHEX analyte flowed through each cell for 6 min. The secPHEX, 6-minute injection pulse is indicated as a line above the sensorgram. A distinct association and dissociation curve occurred with secPHEX analyte and MEPE-immobilized ligand indicating a strong MEPE–PHEX association and binding. There was no secPHEX analyte interaction with IgG ligand and a very low level self-association with PHEX ligand and PHEX analyte (possible very low-level homodimer association).

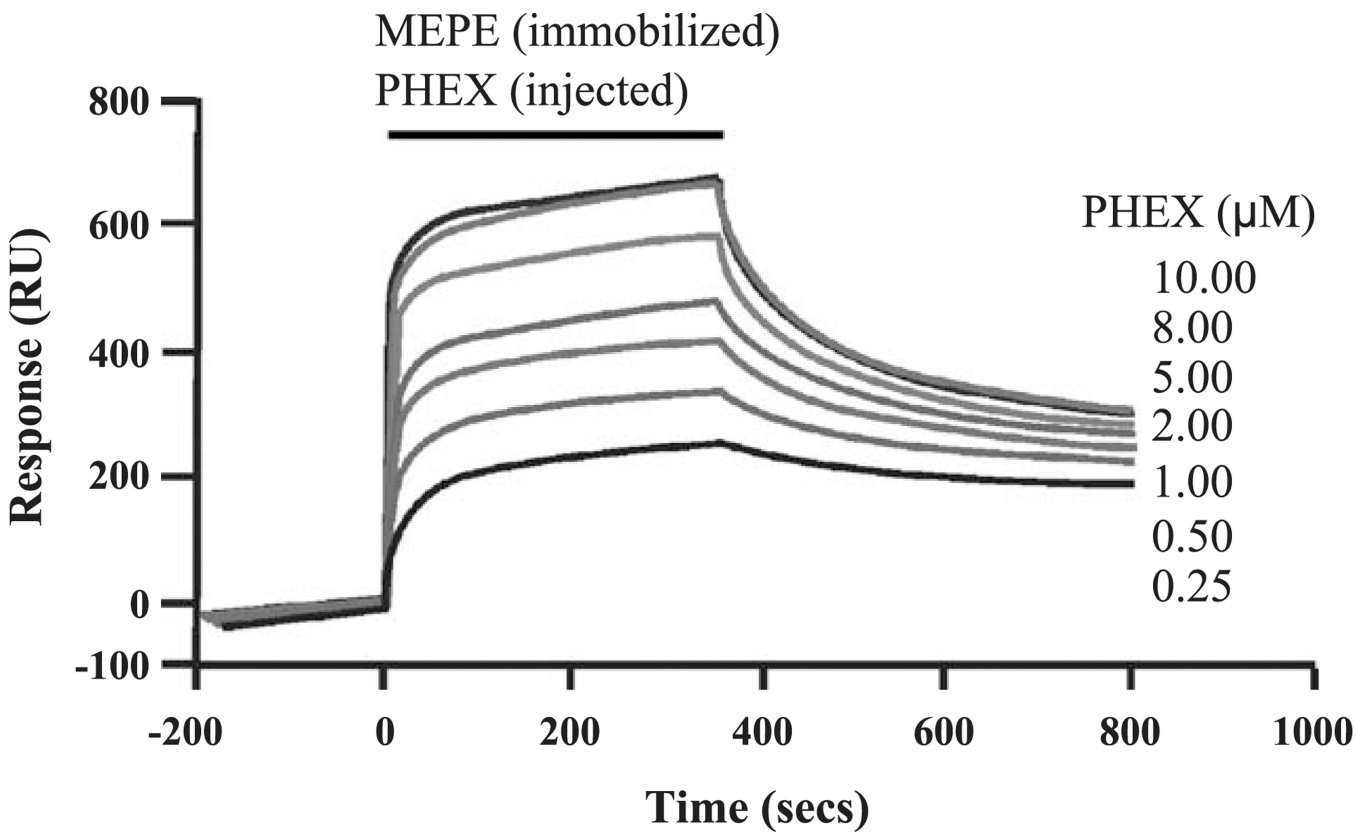

Fig. 2.

Composite Biacore sensorgrams of chip-immobilized MEPE ligand against different concentrations of secPHEX analyte (mobile phase). The secPHEX binding to MEPE is dose-dependent with a distinct plateau or saturation shown at 10 uM secPHEX. The CM-5 chip was coupled with 3500 RU of proteins as indicated in Fig. 1. No interaction was detected with control proteins (IgG) on the same chip (see Fig. 1).

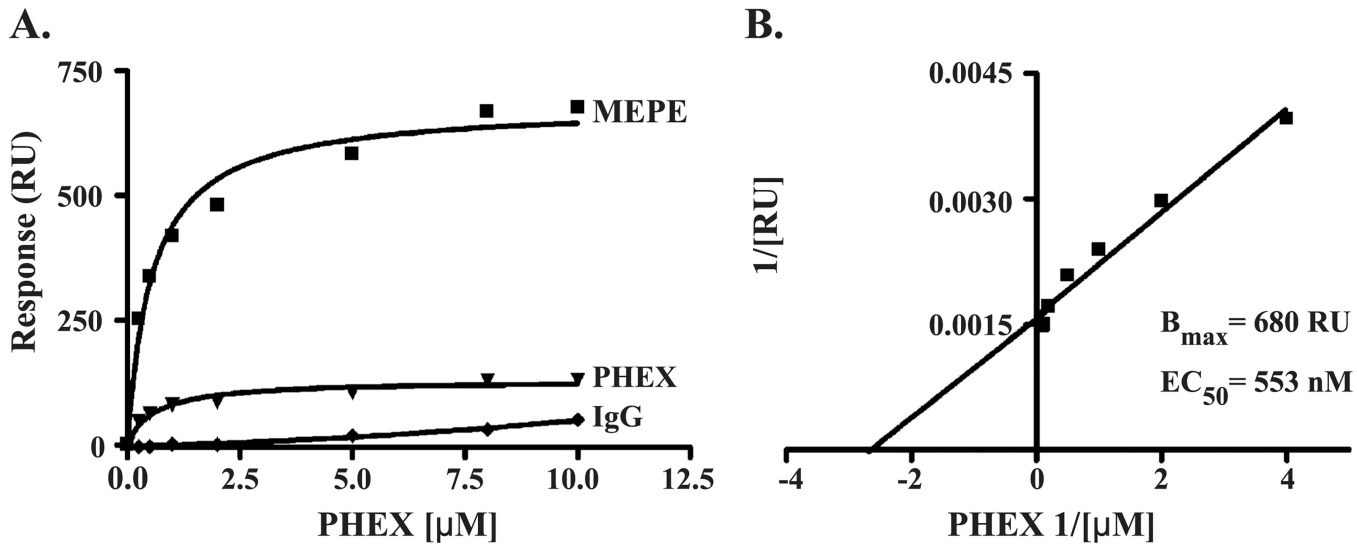

Fig. 3.

Binding of secPHEX to MEPE as calculated from data presented in Figs. 1 and 2. The same coupling of 3500 RU of protein was used. A B_{max} of 680 RU and an EC_{50} of 553 nM were computed for secPHEX (analyte) binding to chip immobilized MEPE (ligand). Graph B presents the binding hyperbola of graph A in linear form by transform plotting of X and Y coordinates as inverse values for secPHEX–MEPE binding. The PHEX–MEPE binding is thus dose-dependent, specific, direct, and saturable.

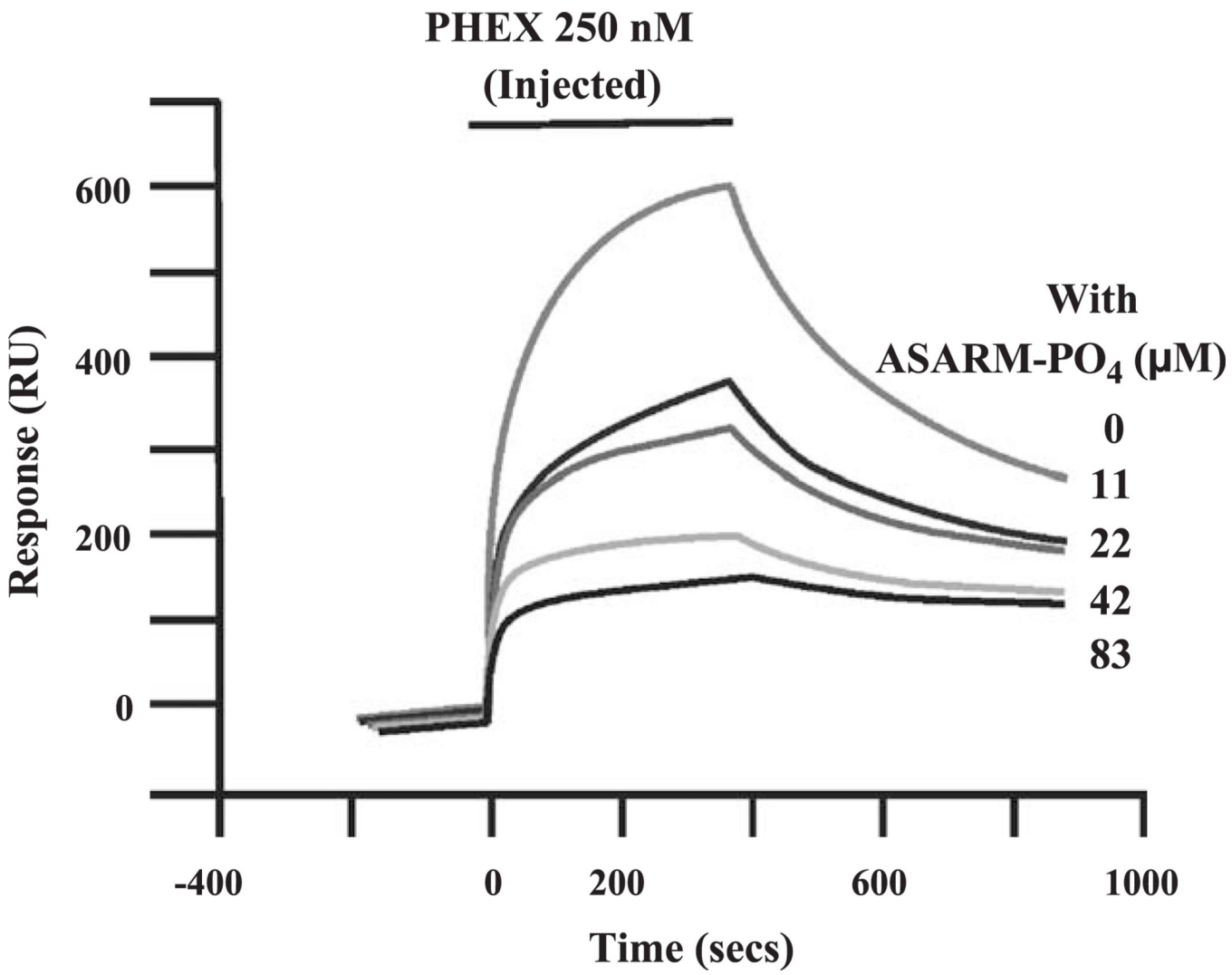

Fig. 4.

Composite PO_4-ASARM peptide competition Biacore sensorgrams of chip-immobilized MEPE ligand against added secPHEX analyte (mobile phase) in the presence of differing concentrations of PO_4-ASARM peptide. The PO_4-ASARM peptide inhibits PHEX–MEPE binding dose-dependently. MEPE ligand was coupled to the chip surface at 6000 RU to increase signal response. PHEX was then injected at a constant 250 nM with a range of concentrations of PO_4-ASARM peptide. Nonphosphorylated ASARM peptide also inhibited secPHEX–MEPE binding but to a lesser extent (see Fig. 5). In contrast, the MEPE–RGD control peptide (see Table 1 for sequences) was completely ineffective at inhibiting secPHEX–MEPE binding at identical concentrations up to 83 uM (see Fig. 5A). This suggests that the ASARM motif plays a role in the secPHEX–MEPE association.

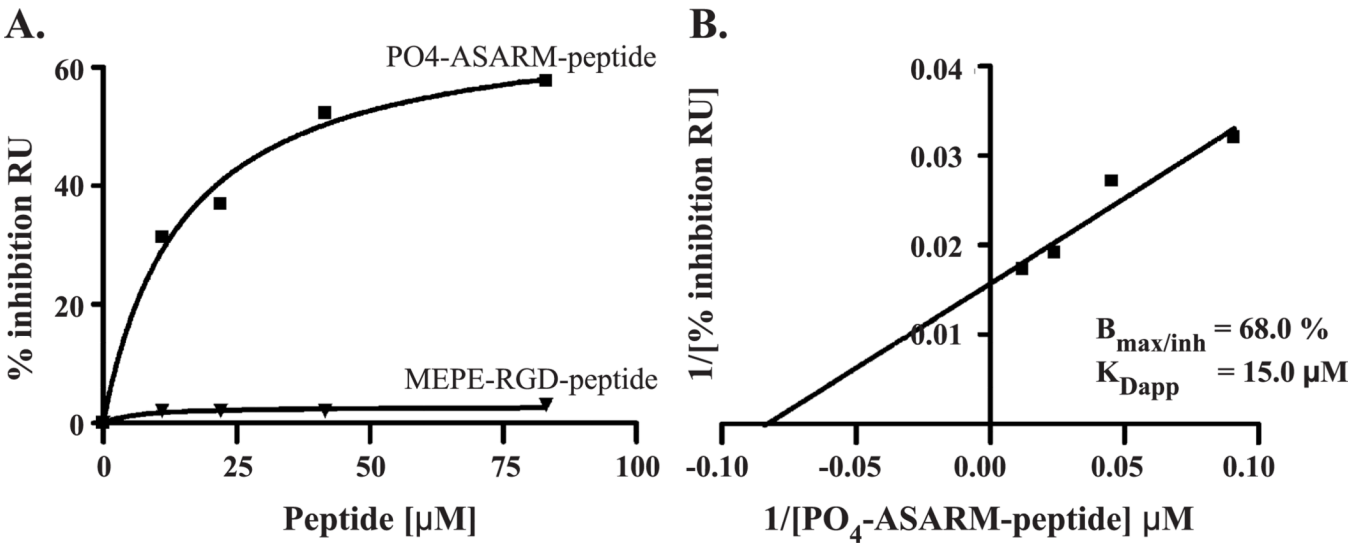

Fig. 5.

Solution competition of secPHEX–MEPE binding in the presence of PO_4-ASARM peptide as calculated from data presented in Fig. 4, with MEPE ligand coupled to 6000 RU. A $B_{max/inhib}$ of 68% inhibition of response units (RU) and an apparent K_{Dapp} of 15 nM were computed. Graph B presents the binding hyperbola of graph A in linear form by transform plotting of X and Y coordinates as inverse values. The $B_{max/inh}$ value represents the maximal peptide-mediated percentage inhibition of PHEX–MEPE binding relative to the "nonpeptide" control (0% inhibition of binding). This was calculated using a constant analyte flow solution of 250 nM secPHEX against immobilized MEPE ligand at 6000 RU. Nonphosphorylated ASARM peptide was less effective at inhibiting the secPHEX–MEPE binding with an approximate K_{Dapp} of 35 uM compared to a K_{Dapp} of 15 uM for the phosphorylated ASARM peptide (PO_4-ASARM peptide). As indicated in Fig. 4, control MEPE–RGD peptide was completely ineffective at inhibiting secPHEX–MEPE binding at identical concentrations up to 83 uM (see A). Moreover, the solution competition of the MEPE PO_4-ASARM peptide was dose-dependent, specific, and saturable. This strongly suggests that the ASARM motif plays a key role in the secPHEX–MEPE association.

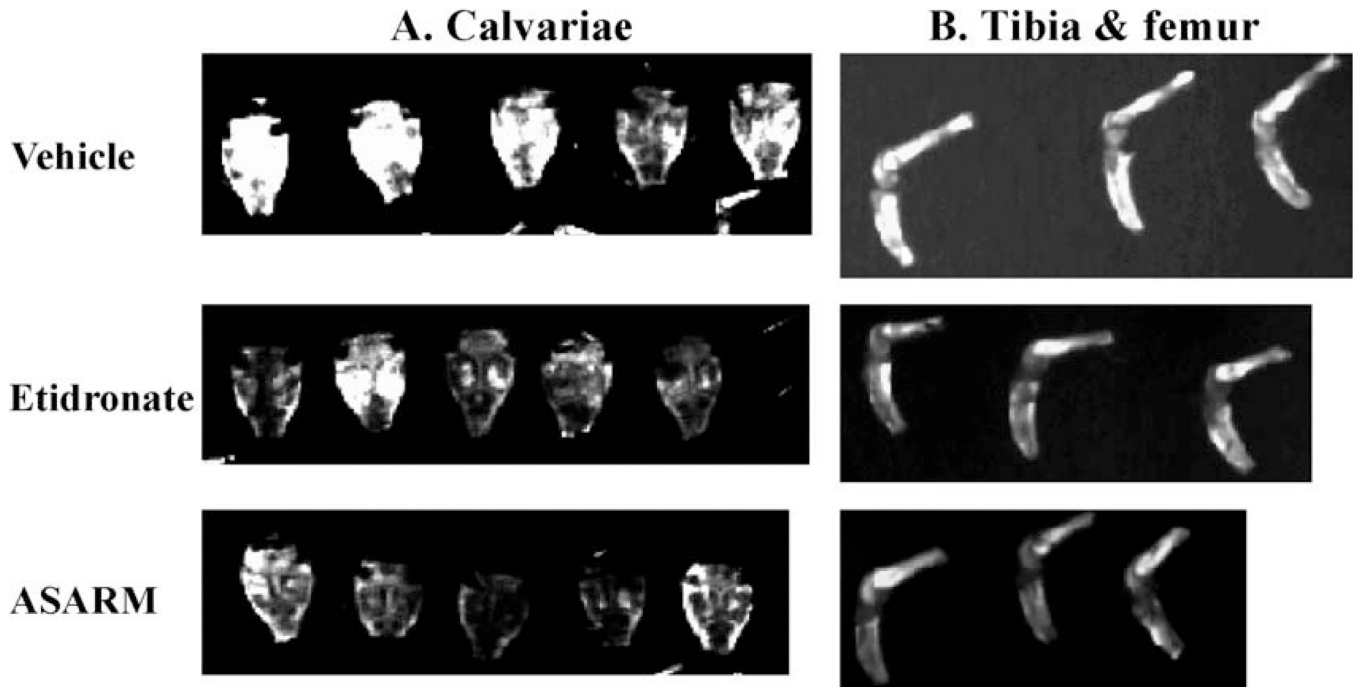

Fig. 6.

Epi-UV fluorescence imaging of undecalcified tissues; (A) calvariae and (B) tibiae and femurs from mice injected with vehicle (HEPES buffer), etidronate (10 mg/kg/day), and PO_4-ASARM peptide (2 mg/kg/day) as indicated. Injections were given once a day for 12 days (except days 6 and 7), and all animals were injected with calcein (20 mg/kg/day) on days 3, 5, 9, and 11, respectively. Samples were imaged simultaneously on a large Bio-Rad imaging platen after epi-UV illumination-induced fluorescence and digital image capture (FluorMax fluor-imager imaging system). Image saturation was avoided by software monitoring (Quantity-1 software) and the captured calcein-fluorescent images quantitated by use of the same software (see Figs. 7A and B). The PO_4-ASARM peptide was massively quenched compared to the vehicle group and even further quenched than the positive control, etidronate. This indicates massive mineralization impairment by the PO_4-ASARM peptide and confirms the effect of etidronate demonstrated previously (references) (see Fig. 7 for fluorescence quantitation and statistics).

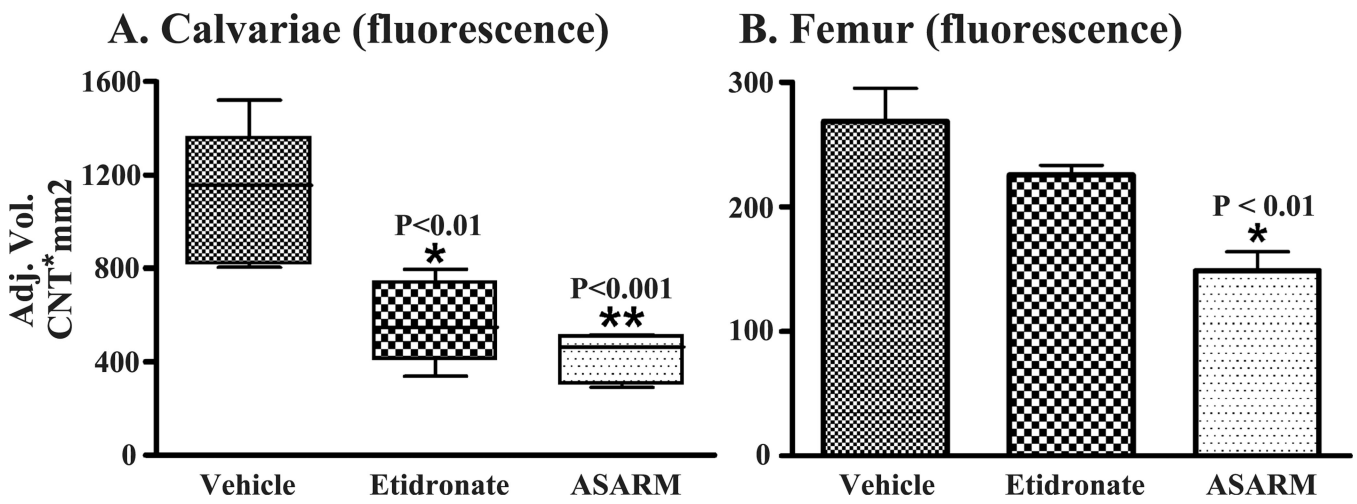

Fig. 7.

Quantitation of whole-fluorescent imaging as depicted in Fig. 6 by use of Bio-Rad Quantity 1 software. Both the PO_4-ASARM peptide and etidronate groups had significant and markedly quenched fluorescence with fluorescent intensity units of 568.7 (SEM = 80.2; N = 5; $P < 0.01$) and 417.7 (SEM = 48.3; N = 5; $P < 0.001$), respectively, compared to the vehicle group at 1100.5 (SEM = 132.8; N = 5). This represents a percentage quenching of 48.4% ($P < 0.01$) for etidronate and 62% ($P < 0.001$) for the PO_4-ASARM peptide, respectively. Graph B illustrates a similar quenching with tibiae-femurs and PO_4-ASARM peptide group fluorescent intensity of 148.9 (SEM = 15.1; N = 5; $P < 0.01$) relative to the vehicle at 268.52 (SEM = 26.8; N = 5). This corresponds to a PO_4-ASARM peptide-mediated fluorescence-signal reduction of 44.5% ($P < 0.01$). Thus, the PO_4-ASARM peptide is an even more effective inhibitor of fluorescence and thus mineralization than the positive control, etidronate.

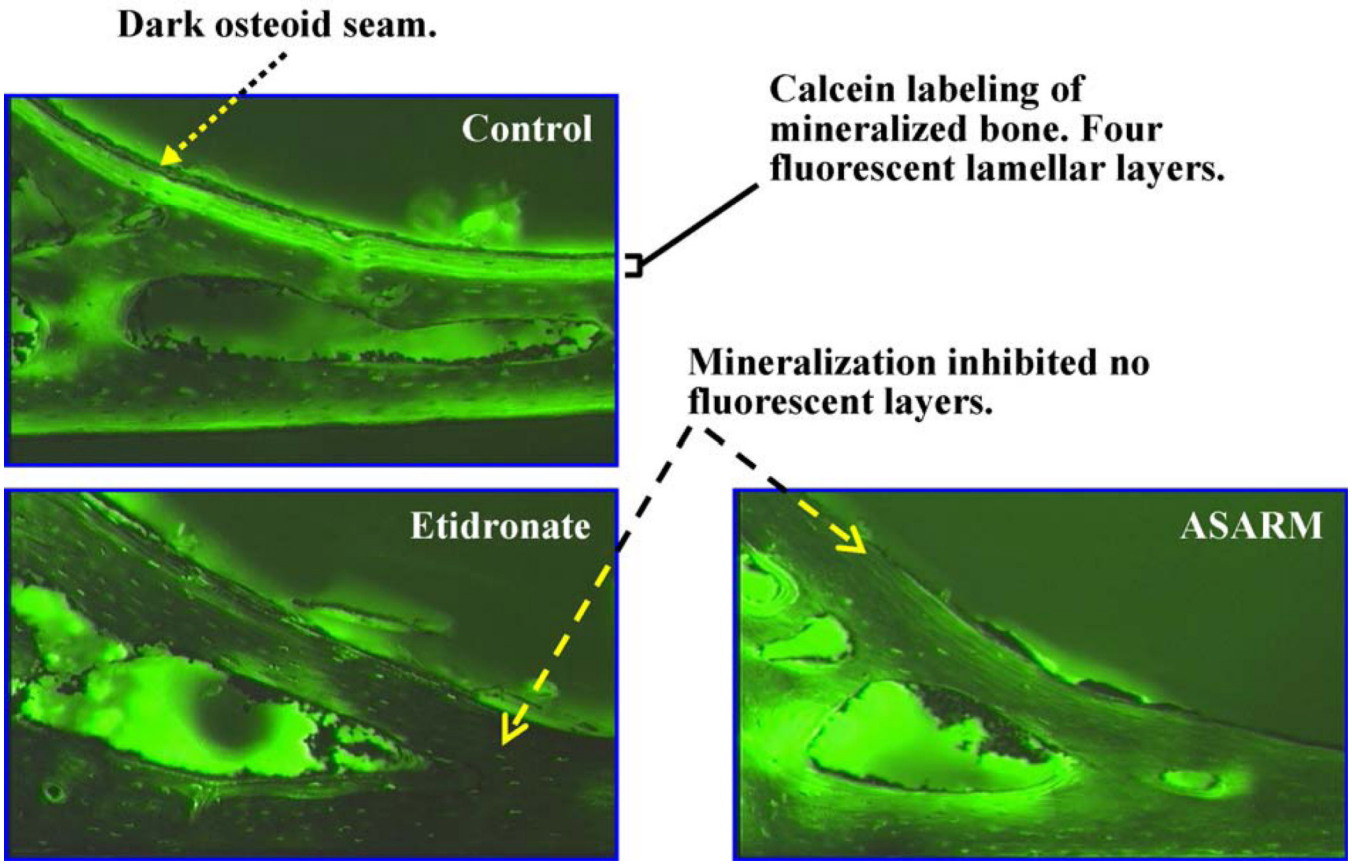

Fig. 8.

Representative photomicrographs of plastic-embedded, undecalcified mice calvariae from Figs. 6 and 7. Slides were analyzed under fluorescent microscope at 200×, and the calcein fluorescence was captured by digital camera. The control group (vehicle) clearly shows four lamellar fluorescent layers corresponding to the four calcein injections (20 mg/kg/day) given on days 3, 5, 9, and 11, respectively. The characteristic and distinct lamellar fluorescent bands were completely absent from the PO_4-ASARM peptide groups as well as in the group treated with etidronate, again indicating impairment of mineralization with the positive control (etidronate) and experimental groups (PO_4-ASARM-peptide).

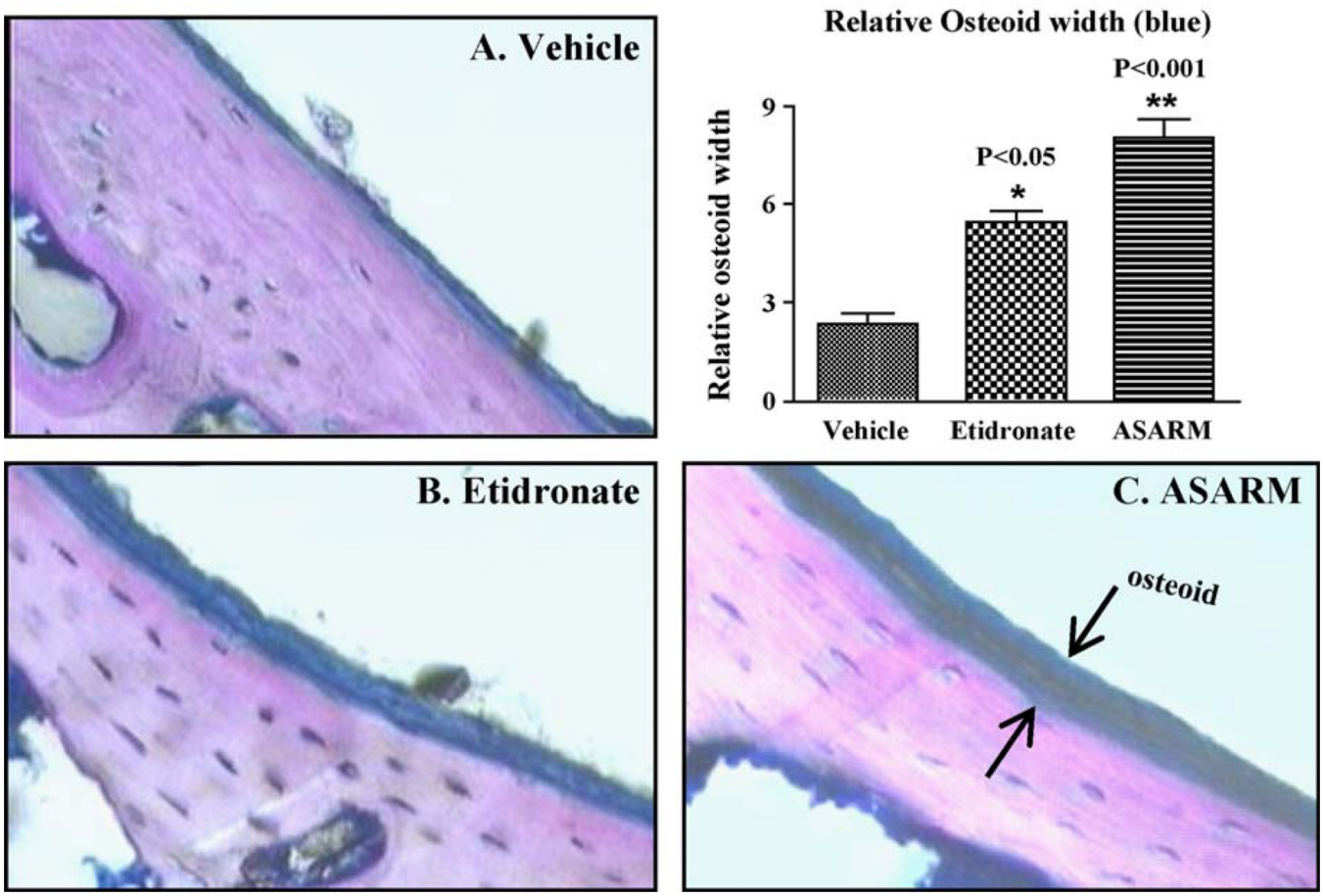

Fig. 9.

Corresponding Sanderson staining of representative mice calvariae, undecalcified cross-sections (×200), embedded in plastic as described for Fig. 8. Mineralized bone stains pink and nonmineralized osteoid stains blue. The darker staining osteoid is clearly visible in grayscale on the upper surface of each sample (A, B, and C) and is highlighted with arrows in C. The osteoid thickness in the etidronate (B) and PO_4-ASARM peptide (C) groups were significantly greater than the vehicle group (A). The inset histogram graphically illustrates the marked increase in thickness and thus impaired mineralization in groups B (etidronate) and C (PO_4-ASARM peptide), with relative thicknesses of 5.4 (SEM = 0.29; $N = 3$; $P < 0.05$) and 8.0 (SEM = 0.57; $N = 3$; $P < 0.001$), respectively, compared to vehicle (A) at 2.3 (SEM = 0.33; $N = 3$). This is consistent with the data shown in Figs. 6, 7, and 8. Measurements were made from the exact same area (suture) in all three groups.

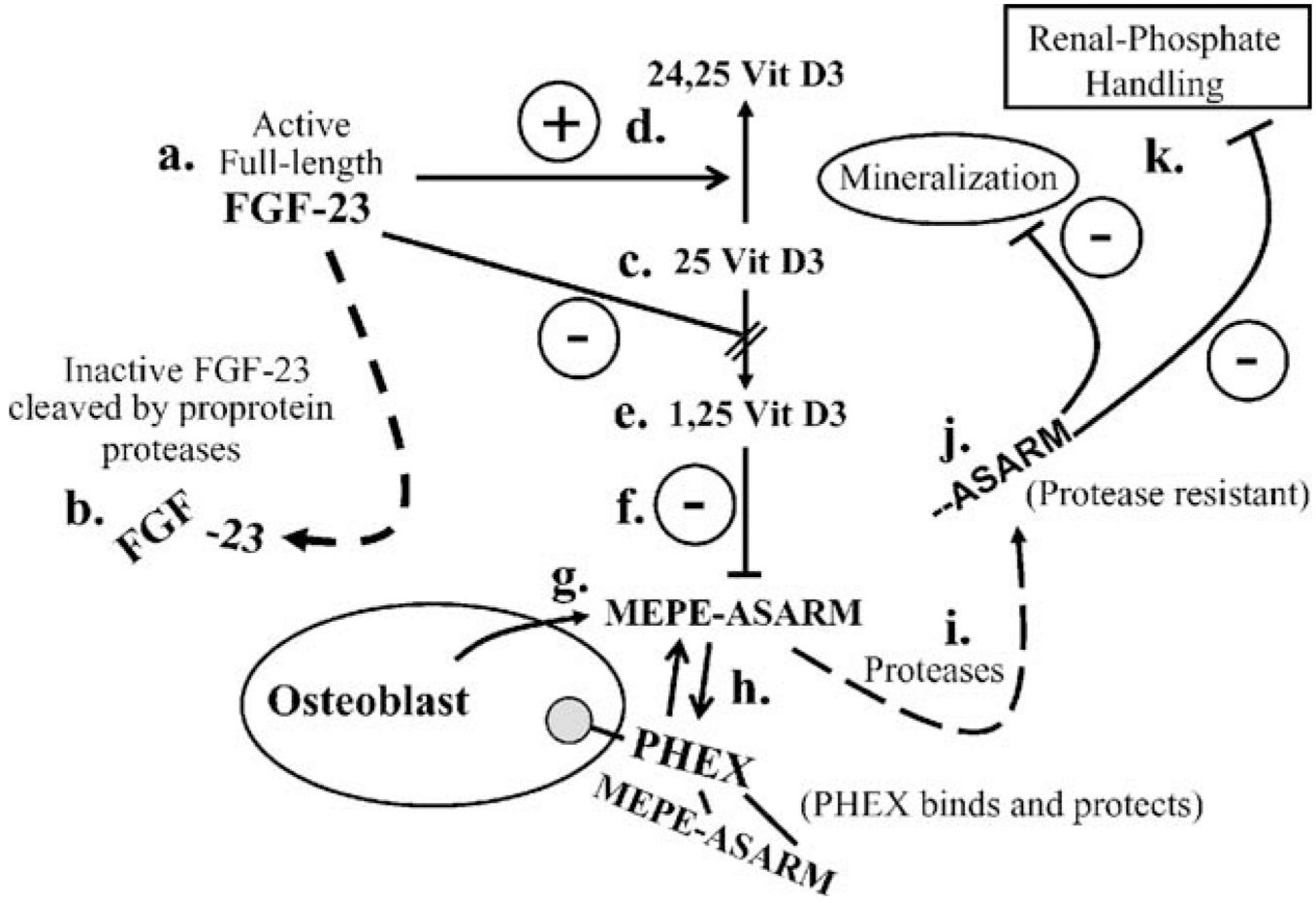

Fig. 10.

This figure depicts a simplified scheme describing the ASARM model. The model is discussed in more detail in a recent review [68]. Also, an animated flash scheme of the ASARM model can be accessed at the following Web site (http://www.periodontics.uthscsa.edu/rowe/asarm-modelandfgf23.html). The letters in the cartoon (a to k) are reference points for text descriptions. Full-length FGF23 is the active form of the molecule. The primary physiological tissue(s) and sites of FGF23 expression are uncertain and could involve bone and/or extraosseous sites (a) [27,39,40,97]. Inactivation of FGF23 (b) is thought to occur through the action of proprotein convertases and not PHEX [4,51]. Autosomal dominant hypophosphatemic rickets (ADHR) is due to activating mutations in FGF23 that increase half-life of the phosphaturic full-length form (a). FGF23 is a potent down-regulator of 1-α-hydroxylase expression (c) and up-regulates the catabolic enzyme 24-hydroxylase (d) [79]. This results in suppression of serum 1,25 vitamin D levels (e) [79]. Indeed, the effects mediated by full-length FGF23 on vitamin D metabolism are more marked than the direct effects on phosphate handling in vivo [79]. Also, 1,25 vitamin D3 suppresses expression of MEPE (f) [2,59,71]. Thus, suppression of 1,25 vitamin D3 levels by FGF23 will in turn increase expression of MEPE (g). We provide evidence in this paper and a previous publication [27] that MEPE reversibly interacts with PHEX, and this interaction protects MEPE from proteolysis (h). Also, the ASARM motif plays a major role in the PHEX–MEPE interaction (h). In Hyp, PHEX is defective [29,70,73] and cannot bind to MEPE and/or protect the molecule from proteolysis. The FGF23 levels in Hyp are elevated, serum 1,25 vitamin D3 is suppressed, osteoblastic MEPE expression is elevated, and the levels of osteoblastic proteases are also markedly elevated (i) [2,3,17,27,32,33,

39,89]. The increased MEPE and protease levels result in increased proteolysis of MEPE and release of the protease resistant ASARM peptide (j). This is compounded by loss of protease protection due to defective PHEX (h). The ASARM peptide in turn inhibits mineralization and renal phosphate handling and is wholly or in part responsible for the hypophosphatemia and rickets/osteomalacia (k). Further evidence for a key MEPE role in phosphate metabolism and mineralization is the finding that MEPE serum levels are 450 ng/ml up to 1.6 Ag/ml in normal subjects, and the levels are tightly correlated with serum phosphorus, PTH, bone mineral density (BMD), and FGF23 [30,39]. Moreover, MEPE is phosphaturic in vivo and in vitro, and the ASARM peptide may play a key role [14,71]. Of additional interest, MEPE expression is down-regulated by FGF2, a cytokine involved in bone formation [98].

Table 1

Sequences and text codes of peptides used for surface plasmon resonance (SPR) and mineralization studies

Peptide region	Sequence	Code in text
MEPE–ASARM peptide (507–525)	RDDSSESSDSG(Sp)S(Sp)E(Sp)DGD	PO_4-ASARM peptide
MEPE–ASARM peptide nonphosphorylated (502–525)	CFSSRRRDDSSESSDSGSSSESDGD	ASARM peptide
MEPE–RGD midregion peptide (238–262)	GSGYTDLQERGDNDISPFSGDGQPF	MEPE–RGD